The NEON 2010 Airborne Pathfinder Campaign in Florida

Thomas Kampe[a], Keith Krause[a], Courtney Meier[a], David Barnett[a], Joel M[c]Corkel[a*]

[a]National Ecological Observatory Network, 1685 38th St., Suite 100, Boulder, CO 80301

ABSTRACT

The National Ecological Observatory Network (NEON) conducted a series of airborne flights and supporting ground measurements in two study areas located near Gainesville, Florida in August and September 2010. The primary objectives of the combined airborne and field campaign were to prototype data collection approaches and to evaluate data processing techniques planned for use in the processing of future NEON airborne remote sensing data. Since the instrumentation slated for deployment on the eventual AOP remote sensing payloads were not yet available, airborne spectroscopic and LiDAR measurements were made during this campaign using existing systems that exhibit similar performance characteristics as the instrumentation under development. Supporting ground measurements of vegetation spectra and structure, plant species identification and key atmospheric variables measurements were made. Ground-based leaf area index (LAI) measurements were made along several 500-meter transects located within the notional airshed of the planned NEON flux tower location in OSBS. Leaf area measurement were also made along six transects in the Donaldson tract. In OSBS, detailed structure measurements were made in a 20x120 meter area along one of the transects. These included measurements of tree height, height to first branch, canopy diameter, stem diameter, and species identification. Plant diversity data were collected in a number of plots dispersed throughout OSBS.

Keywords: Airborne remote sensing, imaging spectroscopy, leaf area index

*Now with NASA Goddard Space Flight Center, 8800 Greenbelt Road, Greenbelt, Maryland 20771

Table of Contents

List of Tables

List of Figures

1 INTRODUCTION

The National Ecological Observatory Network (NEON) conducted a series of airborne flights and supporting ground measurements in two study areas located near Gainesville, Florida in August and September 2010. The primary objectives of the combined airborne and field campaign were to prototype data collection approaches and to evaluate data processing techniques planned for use in the processing of future NEON airborne remote sensing data. The science goals for the airborne system require observations over a wide range of ecosystem attributes ranging from plant functional types, vegetative biochemical and biophysical properties, to regional ecosystem structure and functioning. The airborne instrumentation used by NEON to achieve these goals consists of an imaging spectrometer, a waveform-recording LIDAR and high-resolution digital camera[1]. Producing consistent, high quality scientific data products from remote sensing measurements places demanding requirements on instrument performance and stability, requires regular laboratory calibration traceable to recognized standards and a robust, long-term field validation procedure for assessing the accuracy of the derived products. In addition, linking regional remote sensing measurements to field measurements that capture fine-scale ecosystem processes requires new approaches to data collection and analysis.

The 2010 Airborne Observatory (AOP) Pathfinder Campaign was conducted in Putnam County, Florida, in the surrounding areas near Gainesville, Florida and included two distinct regions. One of the regions studied was the Ordway-Swisher Biological Station (OSBS) and surrounding area. OSBS is the Domain 3 core site for NEON representing the Southeastern United States. The NEON Southeast Domain 3 contains the southern portions of the Gulf Coast states, half of South Carolina, and all of Florida except for the southern tip. OSBS, the core site for Domain 3, is an approximately 37-square kilometer area in Putnam County in north-central Florida and is managed jointly by the University of Florida and the Nature Conservancy. The research focus for the domain is land use, and OSBS anchors the southeastern point in the NEON forest management research gradient that includes companion sites in the Great Lakes (Domain 5) and the Pacific Northwest (Domain 17). OSBS features diverse natural forests, small pine plantations and a range of wildlife species that reflects the area's ecological communities. Nine major plant communities exist within the region as defined by the Florida Natural Areas Inventory and these diverse targets are populated by sandhill, xeric hammock, upland mixed forest, baygalls, basin swamp, basin marsh, marsh lake, clastic upland lake and sandhill upland lakes[2]. The sandhills community is managed using prescribed burning on a scheduled 3-year rotation. The ground-sampling portion of this campaign focused on a sandhill ecosystem dominated by Long-Leaf Pine (*P. palustris*) and Turkey Oak (*Quercus laevis*). The sandhill ecosystem at OSBS was selected for concurrent ground measurements because a NEON instrumented tower will be located within this ecosystem type.

The OSBS covers an area of approximately 9,000 acres consisting of a mosaic of pine forest, wetlands and grass prairie with some portions actively managed using prescribed fire as the primary management tool. OSBS has areas with homogenous forest and prairie communities, and areas of mixed patches of plant communities and vegetation structure making this region well suited for testing the ground validation and processing techniques for NEON over a range of vegetation communities, extending from of simple to complex. The second area surveyed was the nearby Donaldson Tract, which is a managed pine plantation. The plantation was clear-cut and replanted in January of 1990. The even-aged overstory consists of slash pine with an understory of native plant

species. This study area was chosen primarily for validating the airborne LIDAR structure measurements. The locations of these study sites relative to the Gainesville Regional Airport are shown in Figure 1. In addition to Ordway-Swisher Biological Station and Donaldson Plantation, data from over a radiometric calibration site near the Gainesville Regional Airport was also obtained.

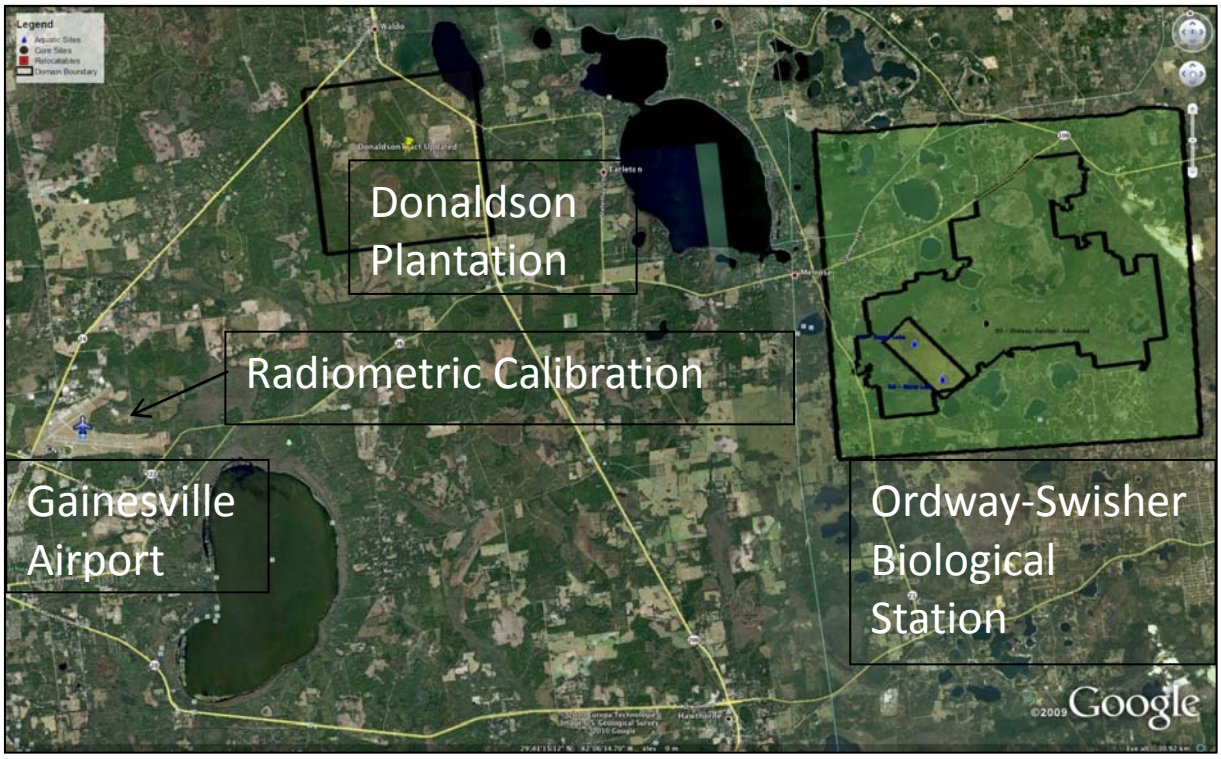

Figure 1. Study areas sampled during the 2010 AOP Pathfinder Campaign.

Since the instrumentation slated for deployment on the eventual AOP remote sensing payloads were not yet available, airborne spectroscopic and LiDAR measurements were made during this campaign using existing systems that exhibit similar performance characteristics as the instrumentation under development. Similar aircraft operating parameters as those envisaged for routine flight operations were also employed. The Airborne Visible/Infrared Imaging Spectrometer (AVIRIS)[3] instrument operated by personnel from the Jet Propulsion Laboratory (JPL) was deployed on a Twin Otter aircraft in partnership with the National Aeronautics and Space Administration Terrestrial Ecology Program. AVIRIS collected low altitude airborne visible, near-infrared and shortwave infrared spectral measurements over the study areas. The National Center for Airborne Laser Mapping (NCALM) conducted flights on a separate aircraft collecting discrete return and waveform LiDAR measurements using their commercial Optech Gemini system.

Supporting ground measurements of vegetation spectra and structure, plant species identification and key atmospheric variables measurements were made. Ground-based leaf area index (LAI) measurements were made along several 500-meter transects located within the notional airshed of the planned NEON flux tower location in OSBS. Leaf area measurement were also made along six transects in the Donaldson tract. In OSBS, detailed structure measurements were made in a 20x120

meter area along one of the transects. These included measurements of tree height, height to first branch, canopy diameter, stem diameter, and species identification. Plant diversity data were collected in a number of plots dispersed throughout OSBS.

In addition to validating the airborne measurements, the collection of coincident field measurements provides a first opportunity to evaluate approaches being developed at NEON for integrating field, site-based, and remote sensing data from across a range of spatial scales. The NEON design is based on a multi-scaled sampling strategy employing systematically deployed ground-based sensors, field sampling, high-resolution airborne remote sensing and integration of national geospatial information[4]. An important aspect of this strategy is the capability to extrapolate relationships between climate variability, land-use changes and invasive species to ecological consequences in areas not directly sampled by the NEON facilities. Airborne remote sensing plays a critical role in the scaling strategy by making measurements at the scale of individual shrubs and larger plants over hundreds of square kilometers. Spatially explicit data from the airborne instrumentation serves to bridge the scales from organism and stand scales, as captured by plot and tower observations, to the scale of satellite based remote sensing[5].

This report describes the airborne and field experiments conducted in Florida during late summer of 2010 as part of the AOP Pathfinder Campaign and presents preliminary research results. These results include operational lessons learned; atmospheric correction results; sensor validation experiment results; and precursor vegetation indices and leaf area index products. It is a NEON policy to provide data sets free of charge to the scientific and general community for use in their own studies. The data from this campaign have been made publically available and can be accessed from the NEON website at http://neoninc.org/pds/.

2 EXPERIMENT LOCATIONS

The 2010 AOP Pathfinder Campaign took place at two areas near Gainesville, Florida. These were the Ordway Swisher Biological Station and Donaldson Plantation. In addition, flights of AVIRIS were also conducted over a temporary radiometric calibration site called the “Driving Pad” at the Gainesville Regional Airport. The locations of these sites relative to the Gainesville Regional Airport were shown in Figure 1. The flight crews used the University Air Center at Gainesville Regional Airport as a base of operations. This is the fixed-based operator that the AOP plans to use during operations for the NEON Southeast Domain (Domain 3).

The NEON Southeast Domain includes the OSBS as a core site and two additional sites, one located at the Disney Wilderness Preserve to the south and the second at the Jones Ecological Research Center to the north, although this pathfinder campaign focused exclusively on the OSBS core site. The aircraft and ground data collection activities occurred between August 30 and September 10, 2010. Ground validation activities were also performed between August 8 and August 20, 2010. Within the OSBS site there are two high-resolution sites that were flown by the waveform LiDAR. These include the NEON Aquatic sites and Ashley Prairie. The Driving Pad turned out to be an excellent test calibration site with a very homogeneous surface and large enough area for our purposes. This site will be evaluated further as a possible secondary vicarious calibration site for the AOP. The locations of the field collection experimental sites are shown in Figure 2 and the location of the radiometric calibration site within OSBS is shown in Figure 3. This calibration site was a 32m

x 48m portion of a clearing whose surface consisted primarily of grass, patches of sand, and an occasional small bush as shown in the figure.

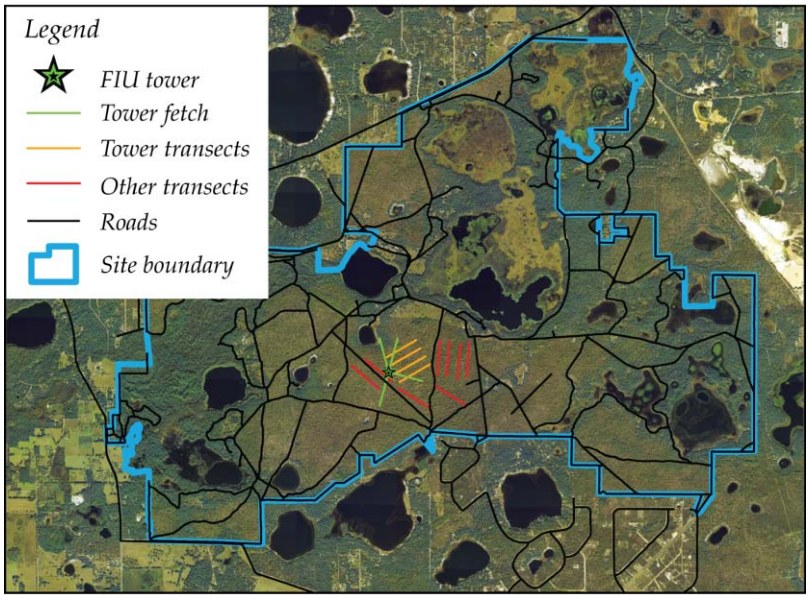

Figure 2. Field measurement locations at the Ordway-Swisher Biological Station.

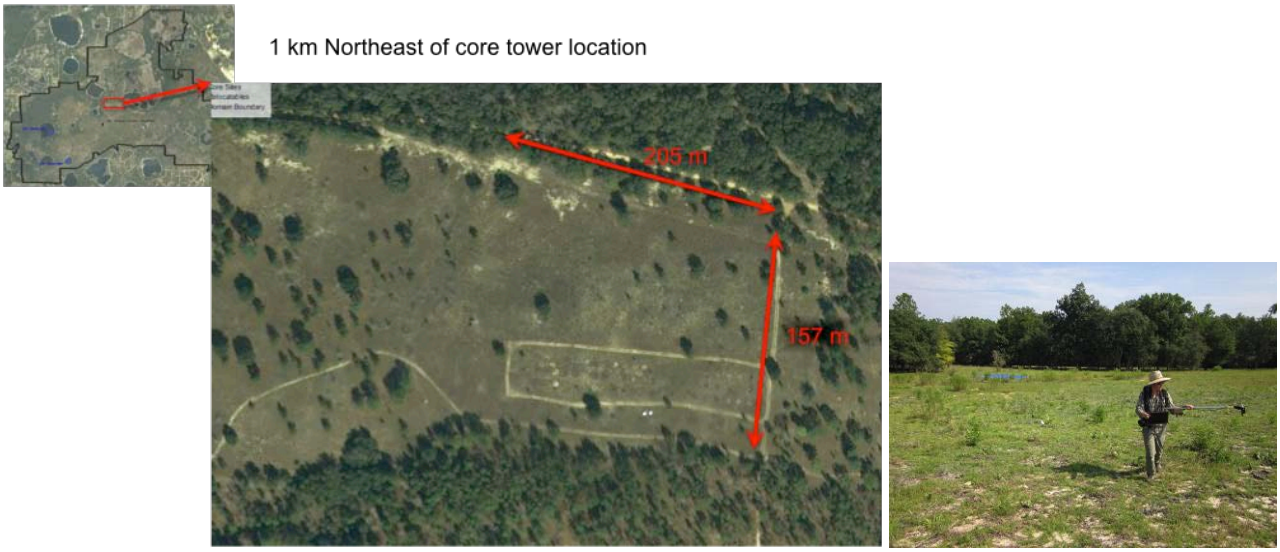

Figure 3. Vegetated radiometric calibration site within the Ordway-Swisher Biological Station.

The primary radiometric test site of the Pathfinder Mission is an aged asphalt lot surrounded by dense evergreen vegetation located nearby the Gainesville Regional Airport. The reflectance measured at this site was found to be fairly flat spectrally, typical of aged asphalt, and is shown in Figure 4. A photo taken at the site in Figure 5 is facing North and depicts a NEON AOP staff member measuring a reflectance standard using a portable spectroradiometer.

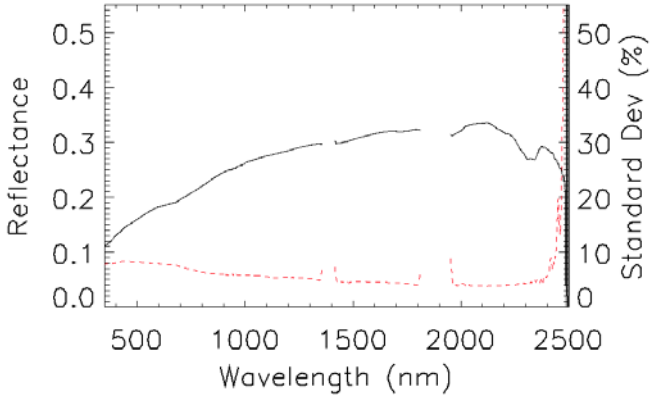

Figure 4. Mean reflectance (black) and percent standard deviation (dashed red) of the asphalt site.

Figure 5. Reflectance reference measurement being made at the southern corner of the asphalt site.

The Donaldson Tract, located within the Austin-Cary Memorial Forest and managed by the University of Florida, was also sampled during this campaign. The site is located 20 km northeast of Gainesville, FL, USA, and is a Slash Pine (*Pinus elliottii*) plantation that was planted in 1965. The understory is composed of saw palmetto (*Serenoa repens*) and galberry (*Ilex glabra*). The Donaldson Tract hosts towered instruments as part of the AmeriFlux Network[6].

3 SCIENTIFIC AND OPERATIONAL OBJECTIVES

A number of scientific and operational questions drove the design of this campaign. These are listed in Table 1 along with the planned experiments designed to address specific questions. Overall, AOP was highly successful in collecting the desired data sets. All desired flight data was collected.

Table 1. Scientific and Operational Questions that drove the Pathfinder Campaign design.

Question	Experiment
Does ground validation data such as LAI change significantly over several weeks?	Sample same LAI transects over a 3 weeks time interval
Can we discriminate individual species with airborne spectral data?	Conduct ground-based spectrometer measurements of known species collected at canopy height. Utilize ground-based spectra for species identification/discrimination in airborne data
How are our reflectance validation measurements affected in a humid environment?	Collect ground-based measurements of reflectance, aerosol optical depth and micrometeorological parameters concurrent with airborne AVIRIS and satellite data (Landsat 5, Hyperion). Evaluate the remotely sensed data (AVIRIS, satellite) against the well-known calibrated ground-based sensors following atmospheric correction
How can we develop an understanding of the scaling issues that NEON will face?	Collect Landsat 4 and 5, MODIS, and EO-1 Hyperion and ALI satellite sensor overpasses during the campaign along with airborne and ground measurements to support scaling studies
How well do various radiometric tools model the atmosphere and will sun photometer and weather station data be used as input or verification of these models?	Collect sun photometer and weather station data along with reflectance data of two ground validation sites
Does solar ephemeris introduce errors in spectrometer data and do uncertainties increase with angle?	Collect airborne spectrometer data during morning and afternoon timeframes along with ground-based data for comparison studies.
What fusion data sets can we explore?	Collect airborne spectroscopic and waveform LiDAR data over both OSBS and Donaldson along with ground measurements. Evaluate the feasibility of creating fused spectroscopic/lidar data even though these products are not collected on the same airborne platforms.

Can ground-based structure measurements be used to validate waveform LiDAR measurements?	Conduct ground and waveform LiDAR structure measurements at Donaldson Plantation as a simple target and OSBS as a more complex target to a) test ground protocols, and b) assess accuracy of lidar discrete and waveform retrievals
What are the uncertainties that arise in waveform LiDAR data with altitude?	Collect waveform LiDAR data at several different altitudes over OSBS during the course of the campaign
Are high-resolution waveform LiDAR data useful for riparian mapping and development of shore input parameters for bathymetry models?	Conduct low-altitude, high-resolution overflights of the NEON Aquatic sites at OSBS with the waveform LiDAR
What information can we get out of a high-resolution waveform LiDAR pass of a region that is scheduled to undergo controlled burning?	Conduct a high resolution (i.e., low-altitude) flight with the waveform LiDAR over Ashley Field in OSBS to obtain a baseline data set. This site will undergo controlled burning in 2011providing the opportunity to conduct a post-burn flight at a later date.
Can we use MODIS aerosol data to improve our atmospheric corrections spatially?	Several MODIS overpass data occurred during the duration of the campaign. Data retrieved from MODIS can be evaluated against the airborne spectroscopic to assess the quality of the atmospheric correction

4 AIRCRAFT DEPLOYMENT

The airborne sensors flown during this campaign were on separate airborne platforms. The AVIRIS instrument was flown aboard a Twin Otter DeHavilland DHC-6-300 aircraft owned and operated by Twin Otter International. The lidar instrument was flown aboard a Cessna 337 Skymaster twin-engine aircraft owned and operated by NCALM. The deployment parameters for lidar and AVIRIS spectroscopic flights are listed in Tables 2 and 3 respectively.

The airborne measurements collected over the OSBS and surrounding region provide an opportunity for NEON to begin development of science data product algorithms for the waveform LiDAR and imaging spectrometer instruments. By mapping the different vegetation types present in this region with the waveform LiDAR, we aim to improve our understanding of measurement uncertainty associated with canopy structure and biomass estimates. By performing these measurements in a well-characterized region with supporting ground measurements, we have the opportunity to conduct direct comparisons to assess and characterize the sources of error in the airborne LiDAR measurements. Sampling vegetation communities, ranging from simple to complex, with the spectrometer alongside ground-based validations allows provides the opportunity for a first look at useful spectral characterization schemes.

Table 2. Pathfinder Campaign waveform LiDAR deployment flight and instrument parameters.

Site	Date	Altitude AGL (m)	PRF (Hz)	Beam Width	Scan Angle (deg)	Scan Freq (Hz)	Digitized Waveform at
Donaldson	9/2	1100	70	Wide	40	40	Every pulse
OSBS	9/1	1500	70	Wide	40	40	Every pulse
NEON Aquatic	8/31	400	125	Narrow	30	60	Every other pulse
Ashley Prairie	9/3	600	100	Narrow	42	40	Every other pulse

The aircraft flew an average 90-knot ground speed during all flights. Flight lines were flown with a 50% overlap.

Table 3. Pathfinder Campaign AVIRIS deployment flight parameters.

Site	Date	Time Start (GMT)	Time End (GMT)	Altitude AGL (m)	Average Ground Speed (kts)
Driving Pad	9/3	2053	2055	3810	66
Driving Pad	9/3	2110	2113	3810	72
OSBS	9/4	1341	1435	3962	83
Driving Pad	9/4	1444	1446	3962	65
Donaldson	9/6	1826	1858	3962	83
OSBS	9/10	1620	1736	3962	76

Flight lines were flown with a 30% overlap.

The OSBS flights were used to collect a NEON-like data set over a NEON site so that we may begin the development of science data product algorithms and explore several operational issues well ahead of the Observatory going operational. A major operational issue is the amount of time available to cover a site. Currently, plans are to fly research sites between 10:00 am and 2:00 pm local time in order to limit the solar angles and keep the Sun high in the sky. This is to limit the amount of shadowing retrieved in the data and increase the intensity of reflected radiation going into the spectrometer and camera measurements. It is also desirable to limit the change in solar angle to limit uncertainties in atmospheric correction. However, during operations, more time may be needed to cover some of NEON's larger sites. It also may be necessary to fly earlier or later in the day in order to avoid cloud decks. Therefore, it was desirable to collect data from two flights flown over the same location at different times of the day. The actual flight lines flown over OSBS by both AVIRIS are shown in Figure 6, while those flown by NCALM are shown in Figure 7.

Figure 6. JPL AVIRIS flight ground tracks for OSBS on September 10, 2012.

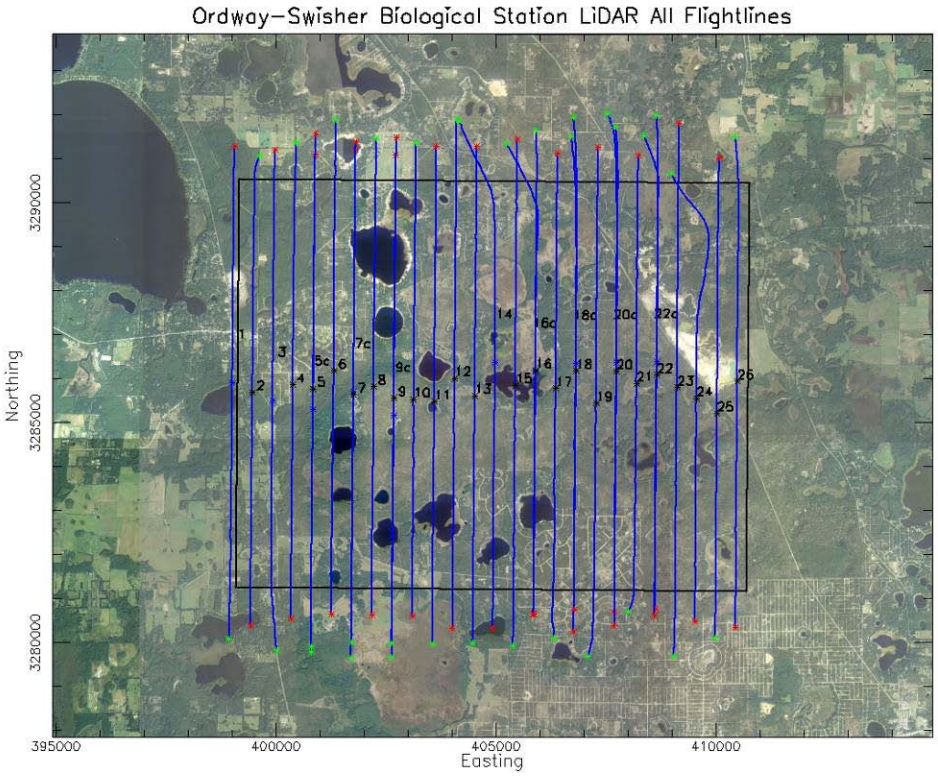

Figure 7. NCALM LiDAR flight ground tracks for OSBS on September 1, 2010.

The high-resolution LiDAR flight tracks flown over the OSBS Aquatic sites on August 31, 2010 are shown in Figure 8. Waveform LiDAR data of NEON Aquatic sites acquired at higher resolution than typical operations can be useful for planning ground operations and potentially aiding the aquatic science by providing elevational information on the riparian areas surrounding lakes, ponds, and other aquatic systems. These data may also input parameters on the shoreline useful for bathymetry models. In order to get a good grasp of the growth in the uncertainty of LiDAR returns with aircraft altitude, several elevations were flown during this campaign. A color height mosaic derived from the Optech discrete return LiDAR data is shown in Figure 9.

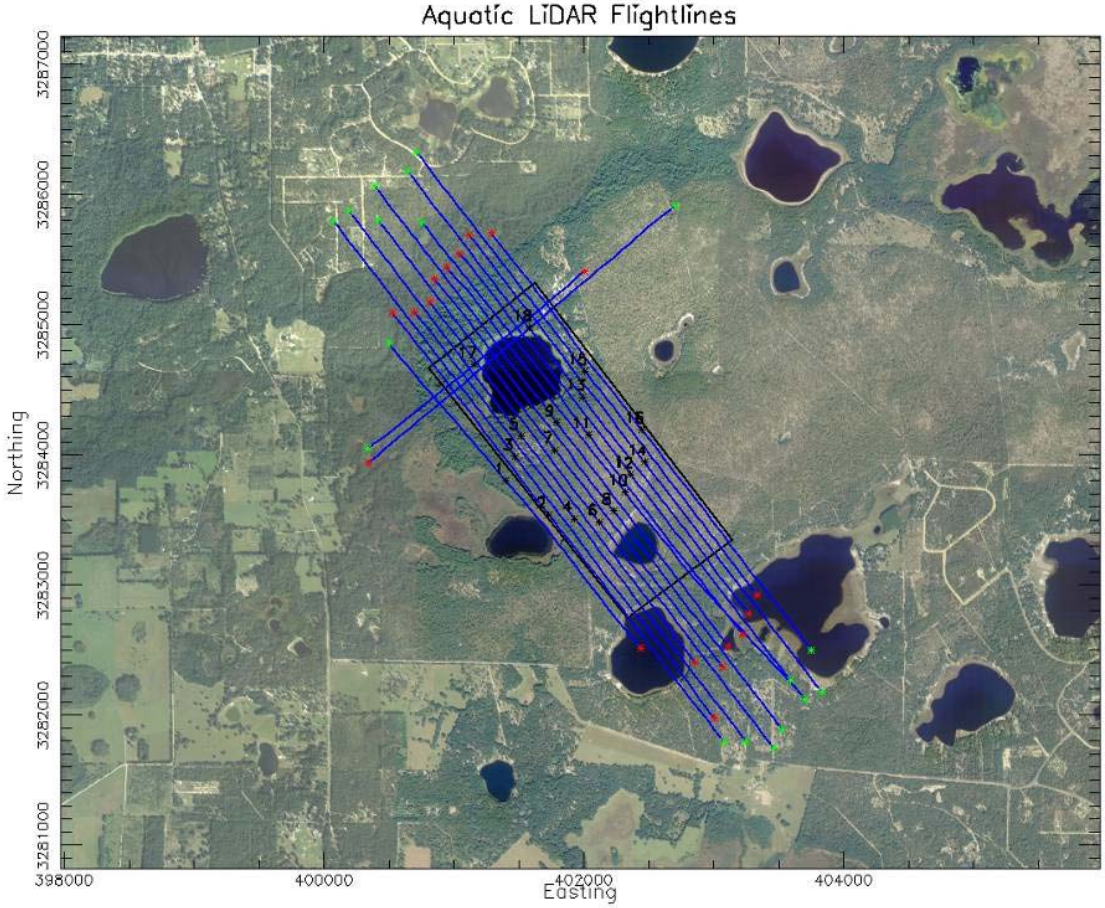

Figure 8. NCALM LiDAR flight ground tracks, Aquatic sites, August 31, 2010.

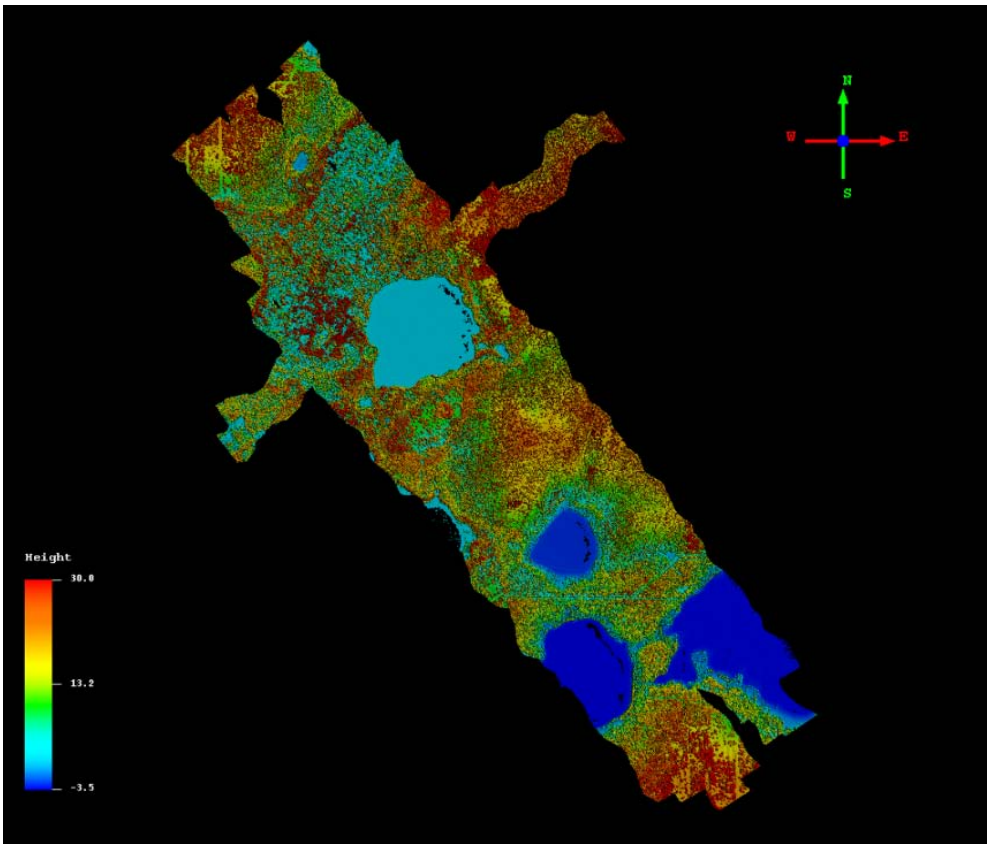

Figure 9. NCALM Optech Gemini LiDAR color height mosaic, Aquatic sites 8/31/10

The waveform LiDAR was flown over Ashley Prairie within OSBS on September 3, 2010. The flight lines are shown in Figure 10. This was a high resolution flight, with the aircraft flying at 600 m AGL. There was interest in obtaining high-resolution lidar data over this region since the Ashley prairie will undergo controlled burning in the spring of 2011 and this would provide an interesting "before-burn" collection of vegetation structure. Instrument parameters include a 100 kHz PRF, 21 deg half scan angle and 40 Hz scan frequency. Digitized waveform data was collected for every other fired laser pulse. A color height mosaic derived from the LiDAR data is shown in Figure 11.

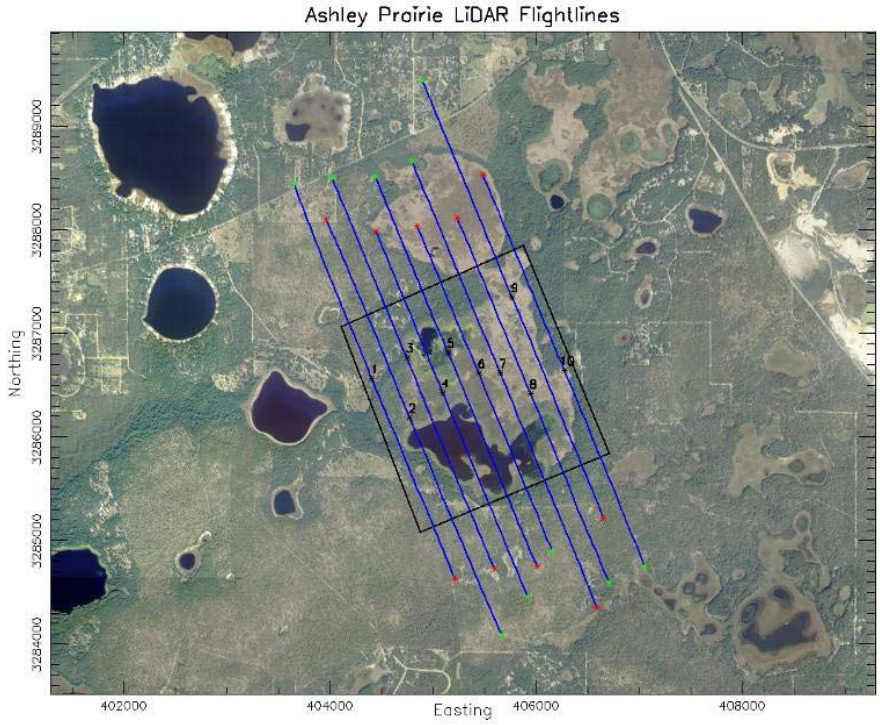

Figure 10. NCALM flight ground tracks of Ashley Prairie, OSBS on September 3, 2010.

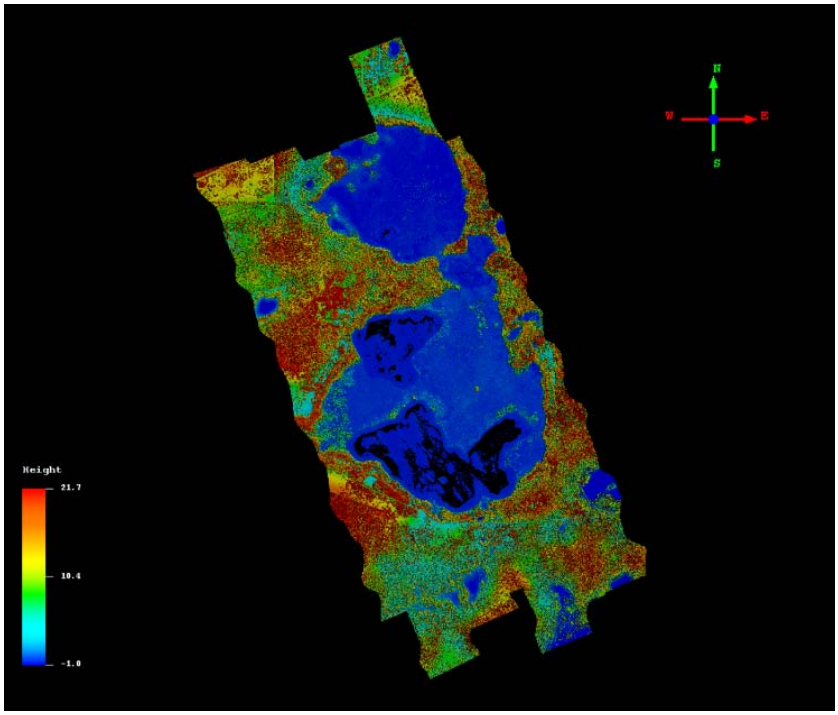

Figure 11. NCALM Optech Gemini LiDAR color height mosaic, Ashley Prairie, OSBS, 9/30/10

On September 2, 2010, the waveform LiDAR was flown over the Donaldson Tract Slash Pine (*Pinus elliotti*) plantation, an area of pine trees of similar age and therefore similar height and spread. This managed pine plantation was selected in order to develop validation techniques for the waveform LiDAR data return in a relatively uniform and well-known region. During this flight, 17 flight lines were collected over the site (Fig. 12). The aircraft was flown at 1100 m AGL with the following instrument parameters: 70 kHZ PRF, a wide beam divergence of 0.8 mrad, 20 deg half scan angle, and 40 Hz scan frequency. Digitized waveform data was collected for every fired laser pulse. A color height mosaic derived from the discrete return LiDAR data is shown in Figure 13.

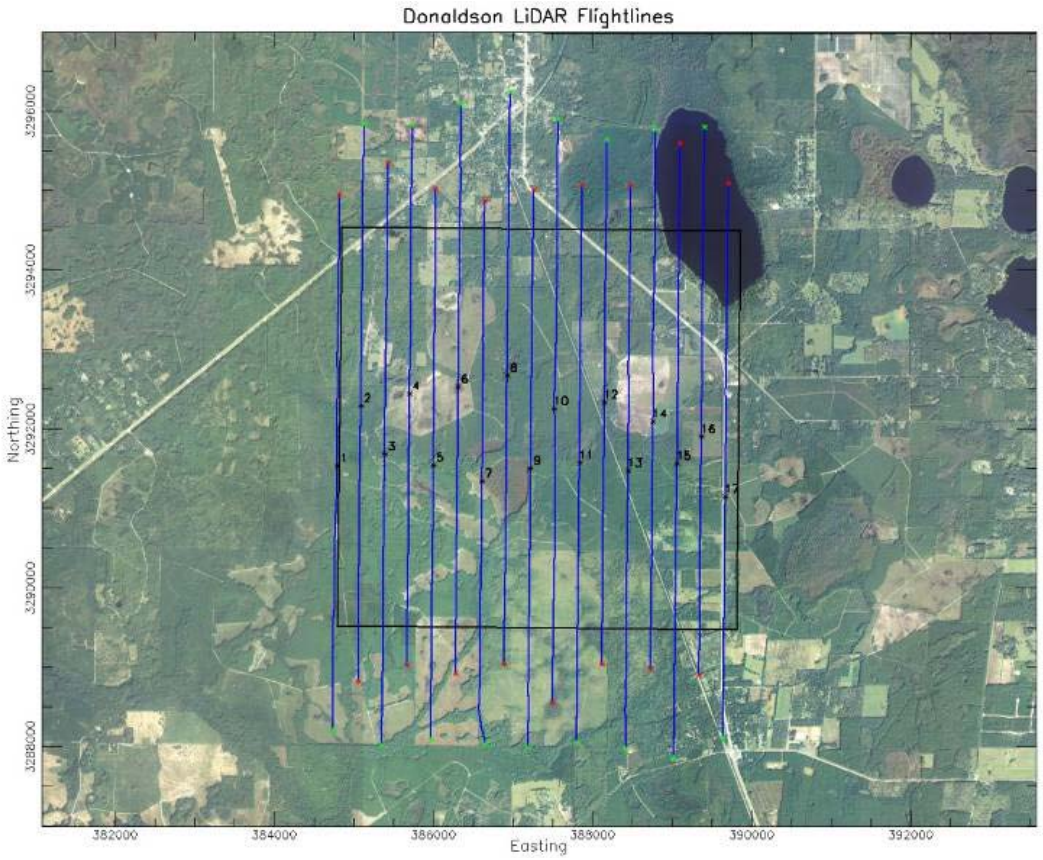

Figure 12. NCALM Optech Gemini LiDAR flight ground tracks, Donaldson Plantation, 9/02/10

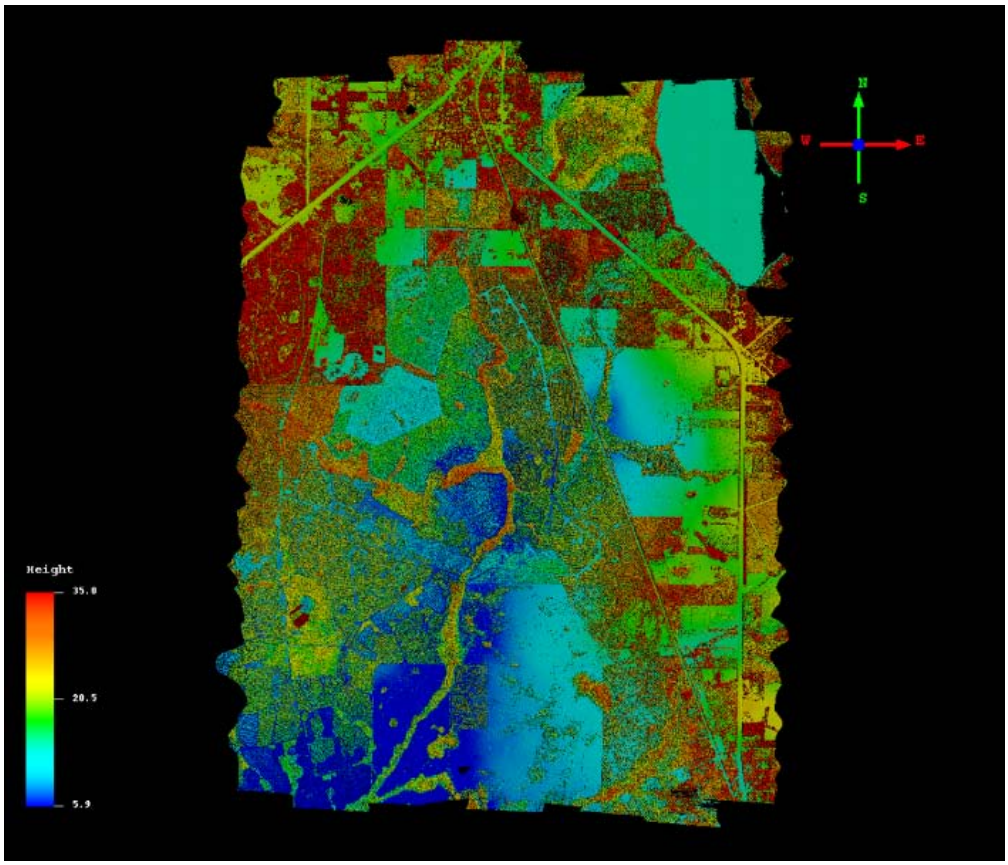

Figure 13. NCALM Optech Gemini LiDAR color height mosaic, Donaldson Plantation, 9/02/10

On September 6, 2010, the AVIRIS instrument was flown over Donaldson Plantation. The twin Otter aircraft flew at approximately 4000m AGL and 90 knots. Three flight tracks were flown as shown in Figure 14. A true color mosaic from Donaldson Plantation derived from the AVIRIS data is shown in Figure 15.

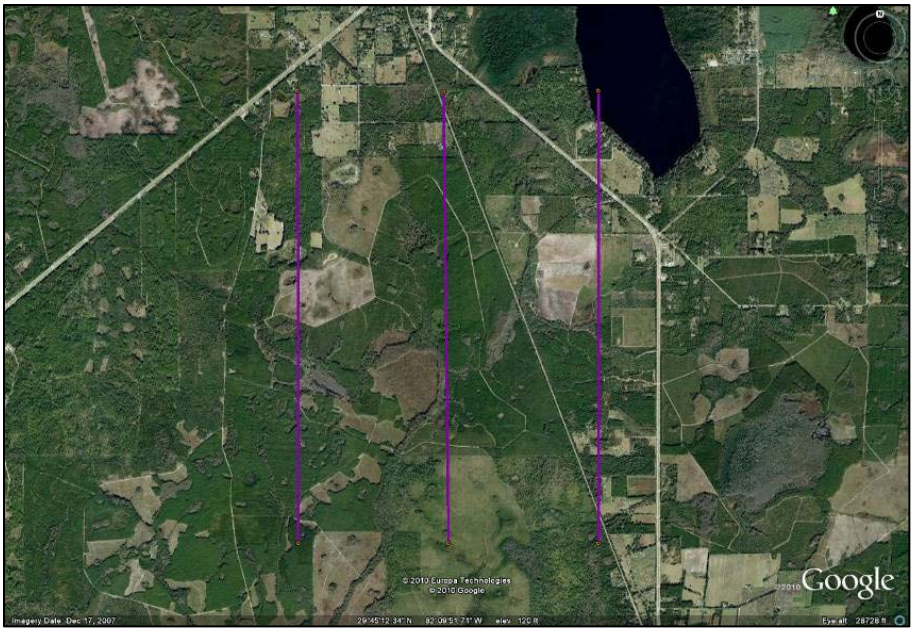

Figure 14. JPL AVIRIS flight ground tracks, Donaldson 9/6/10

Figure 15. JPL AVIRIS true color mosaic, Donaldson Plantation, 9/06/10

The Driving Pad radiometric calibration site, a 240m x 120m aged asphalt lot surrounded by dense evergreen vegetation located nearby the Gainesville Regional Airport, was overflown by AVIRIS on September 4, 2010. The site is centered at 29.695°N latitude and 82.261°W longitude with the long dimension 135° from North. It is a flat surface and the primary use of the lot is motorcycle and automobile training. An overhead view of the Driving Range is shown in Figure 16. The reflectance of the site is fairly flat spectrally, typical of aged asphalt, and was shown in Figure 4. Originally we had planned to fly AVIRIS over this site on September 2, 2010 with the goal of acquiring a coincident acquisition of the site with Landsat 5 TM (Fig. 17) and AVIRIS, but unfortunately due to delay in the aircraft arrival, the September 2 overflight occurred five hours after the Landsat overpass and by then the site was clouded (Figure 18). The AVIRIS instrument was delayed due to extended acquisitions in the Gulf of Mexico due to the Blue Horizon's oil spill disaster.

Figure 16. The "Driving Range" site near the Gainesville Regional Airport (Left). The aged asphalt site is the white rectangle near the center of the image. On the right is the "Driving Range" as observed from AVIRIS on September 4, 2010 at 14:45 UTC.

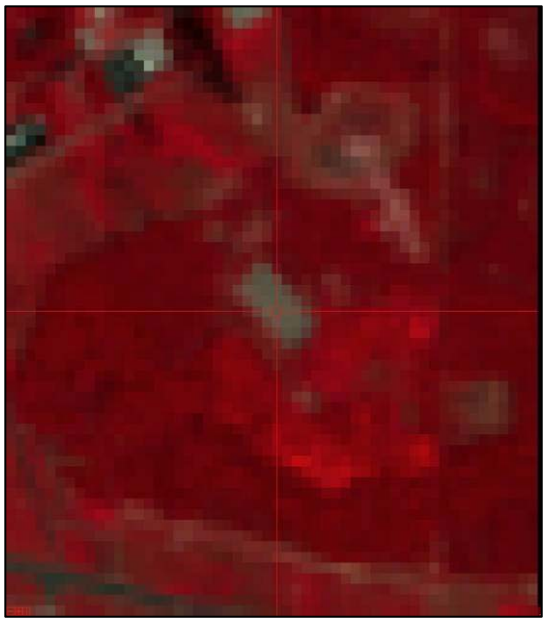

Figure 17. Landsat 5 TM acquisition of “Driving Range” on September 2, 2010 15:51 UTC. The aged asphalt site is the grey region in the center of the image.

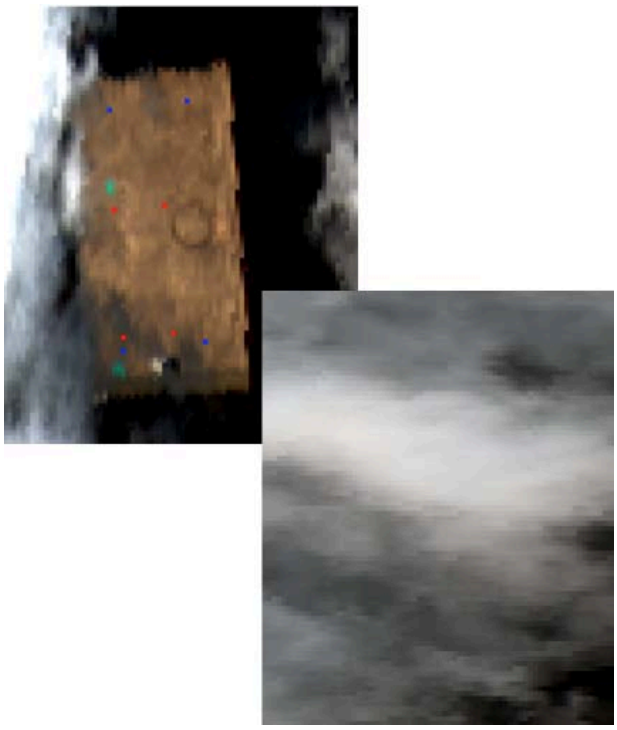

Figure 18. Clouded AVIRIS images of asphalt site on 2 September 2010 at 20:53 and 21:10 UTC.

5 FIELD SAMPLING GOALS AND METHODS

Between the 9th and 20th of August, 2010, field teams collected ground data at both OSBS and the Donaldson Tract within the Austin-Cary Memorial Forest managed by the University of Florida. The primary goals associated with these ground collections were to: 1) develop field training and data collection protocols; 2) collect ground-based data useful for validation of remotely-sensed data collected by the NEON airborne sensors from the same land area; 3) better constrain the time-frame in which ground data must be collected for airborne data validation purposes; 4) collect data capable of informing the ground sampling design – i.e. optimizing plot/transect number, shape, size, and spacing; 5) collect data required for prototyping creation of a plant biomass map of the OSBS site; 6) prototype plot design for optimally measuring plant biodiversity within diverse ecosystem types; and 7) collect ground data that will enable an initial assessment of whether airborne data can be used to monitor for presence and abundance of invasive species.

NEON staff and field crew members collected Leaf Area Index (LAI) and vegetation structure data from two distinct forest ecosystems: The Donaldson Tract Slash Pine (*Pinus elliottii*) plantation and a Sandhill ecosystem dominated by Long-Leaf Pine (*P. palustris*) and Turkey Oak (*Quercus laevis*) that overlaps the proposed tower footprint at the Domain 3 Ordway-Swisher core site. The Donaldson Tract, a managed pine plantation, was selected in order to develop calibration techniques using AOP and FSU data within the context of a structurally simple ecosystem. The sandhill ecosystem at Ordway-Swisher was selected since it is the NEON Core Site, and the FIU tower will be located within this ecosystem type. The locations of the LAI and vegetation structure transects at OSBS are shown in Figure 19; yellow transects lie within the putative NEON tower footprint, and red transects are in Sandhill vegetation but not within the tower footprint. Transects at the Donaldson Plantation are shown in Figure 20.

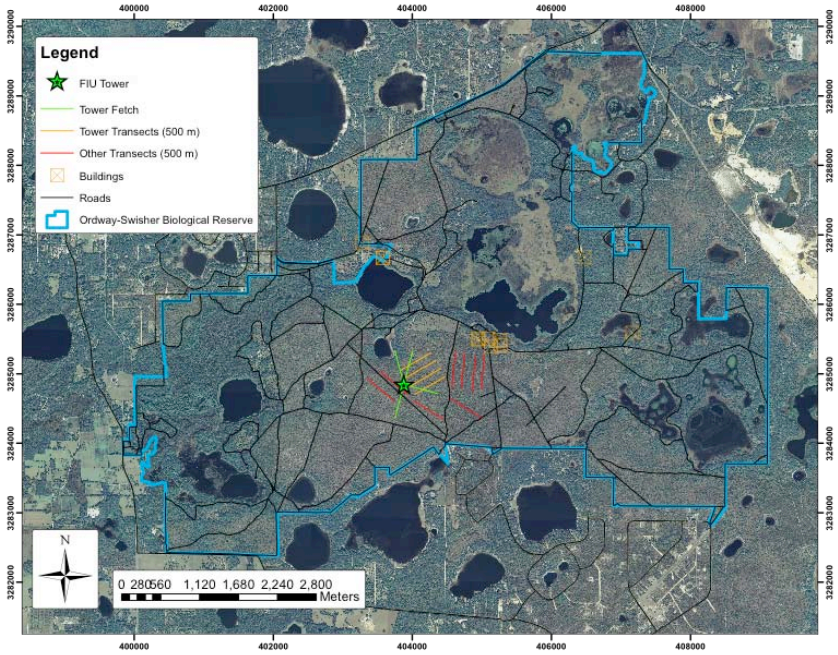

Figure 19. LAI and vegetation structure sampling regions at OSBS.

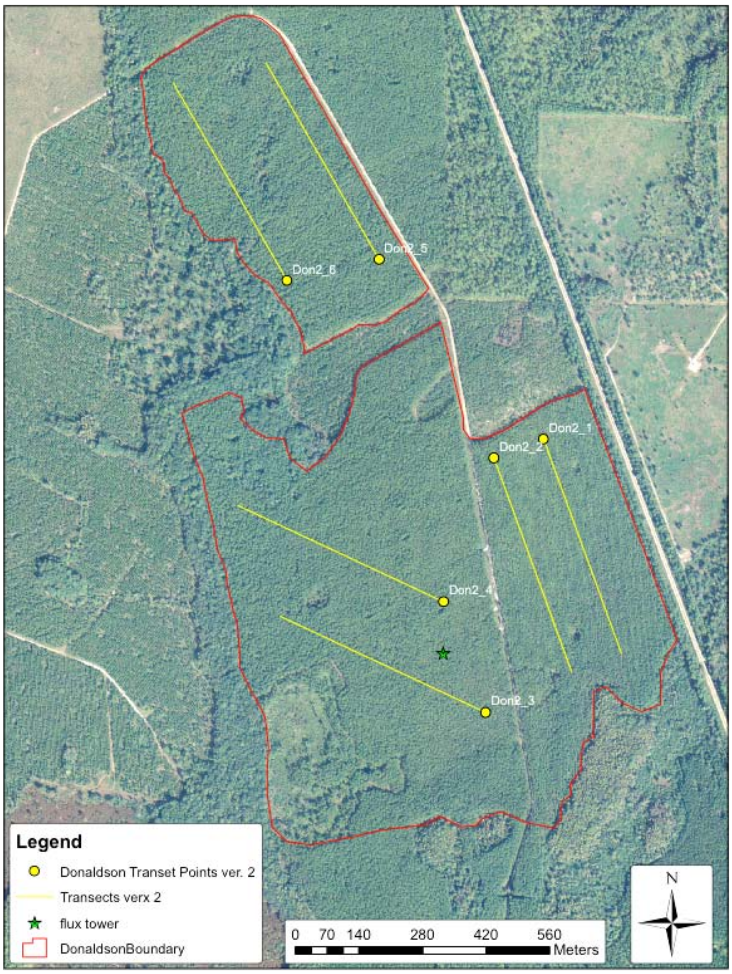

Figure 20. LAI and vegetation structure sampling regions at the Donaldson Plantation.

Transects for measuring LAI and vegetation structure were established at these two field sites. LAI data were collected from 6 transects at the Donaldson Tract on August 10, 12 and 13, and from 8 transects at OSBS on the August 12, 14, 15, and 17. Measurement of LAI occurred during pre-dawn and dusk time periods, corresponding to 6:15–7:15 and 19:45–20:30 local time using both a LiCOR-2200 (Figure 21) and a digital hemispherical photography (DHP) method (Figure 22). Two LAI-2200 instruments were used simultaneously to collect LAI data from parallel transects during a given measurement period. Data were collected from each transect with two-person teams, and above-canopy reference data were collected with a third LAI-2200 wand mounted on a tripod in a clearing located between 0.4 km and 1.5 km from the LAI transects. Each transect was 500 m long, and LAI was recorded at 10 m intervals, with the LAI-2200 instrument held at least 2 m above the soil surface. We compared the LAI-2200 instrument with a DHP system using two transects from the Donaldson Tract, and one transect at OSBS. The purpose of the comparison was to determine whether the increased processing time associated with analyzing DHP images is potentially offset by the benefits of not requiring an above-canopy reference data source, the ability to produce a visible data record (as opposed to only .txt file outputs), and the ability to tag images with GPS metadata.

Figure 21. NEON Staff conducting LAI Measurements using the LICOR LAI-2200.

Figure 22. Digital hemispherical photographs of Long-Leaf Pine canopy (upper) and understory (lower) taken along one of the OSBS transects.

Vegetation structure datasets were collected from both the Donaldson Tract and OSBS between the 11th and 13th of August, 2010. Almost 400 individual shrubs and trees were identified to species, geo-referenced, and measured for a suite of vegetation structure variables, including diameter at breast height, height, and canopy diameter.

Plant biodiversity data were collected using two different-sized, nested plot designs in order to better understand effects of plot-design on required field crew hours, as well as the ability to confidently census plant biodiversity. Between August 14th and 20th, plant diversity data were successfully collected from nine relatively large 1000 m^2 plots, and thirty-nine smaller 168 m^2 plots. Results from preliminary analyses suggest that while larger plots require significantly more time than smaller plots to survey for plant species richness (~45 minutes longer), the extra effort may be worthwhile in the relatively diverse forested plant communities at this site.

A table summarizes the field measurements made during this campaign is shown below.

Table 4. Ground measurements made in the field during the pathfinder flight campaign.

Parameter(s) Measured	Instrument & Measurement Method	Location	Date
Leaf Area Index (LAI)	LiCOR 2200	Donaldson Plantation, OSBS	8/10, 12 & 13 8/12, 14, 15 & 17
Vegetation structure Diameter at breast ht., height and canopy width	Standard forestry tools	Donaldson, OSBS	8/11-13
Plant Biodiversity	Visual census	Donaldson, OSBS	8/14-20
Aerosol Optical Depth (AOD)	Cimel Sun Photometer	OSBS	8/31, 9/1 & 4
		Gainesville Regional Airport	9/2 & 3
Temperature, pressure, wind speed and direction, relative humidity	Kestrel 4500 Pocket Weather Tracker	OSBS	8/31, 9/1 & 4
		Gainesville Regional Airport	9/2 & 3
Spectral reflectance of various plant species (400-2500 nm)	ASD FieldSpec 3	OSBS	8/31, 9/1 & 4
Spectral reflectance of calibration target (at 400-2500 nm)	ASD FieldSpec 3	Gainesville Regional Airport	9/3 & 4
GPS base station location	Trimble R5	2 separate locations within OSBS	8/31

6 GROUND CALIBRATION OF REMOTE SENSING EQUIPMENT

In addition to the airborne and field measurements, a suite of ground measurements were conducted. This suite of measurements included atmospheric characterization using a Cimel sun photometer and a weather station; highly accurate measurements of latitude, longitude, and altitude at three locations using precision Trimble R5 GPS base stations; ground-based and canopy-top spectral measurements of vegetation; and measurements of surface reflectance at well-characterized calibration sites. These ground-based efforts took place during the two weeks of the actual flights, extending from August 31, 2010 to September 10, 2010 at OSBS, the radiometric calibration site at the Gainesville Regional Airport, and the Calibration Site at OSBS. The primary goals associated with these ground collections were to: 1) develop field training and data protocols; 2) collect atmospheric characterization data for atmospheric correction of the spectrometer data; 3) prototype experiment design and collect ground-based data useful for the validation of the laboratory radiometric calibration of the airborne sensors; 4) better constrain the time-frame in which ground data must be collected for airborne data validation purposes; 5) prototype spectral measurements of canopy tops at the ground with the use of an aerial boom lift; and 6) collect several GPS base station measurements to determine the need for additional base station measurements to the NOAA CORS network when applying corrections to aircraft GPS data.

6.1 Atmospheric Characterization

Atmospheric characterization relied on measurements of a CIMEL sun photometer in coordination with the NASA Aerosol Robotic Network (AERONET)[7]. Cimel sun photometer, shown in Figure 23, is a ten spectral channel radiometer designed to measure solar irradiance and sky radiance. The spectral channels span the visible to near-infrared portion of the solar-reflective spectrum and are specifically located at 340, 380, 440, 500, 675, 870, 1020, and 1640 nm (The unit utilized during the Pathfinder mission had a non-traditional 1200 nm channel instead of the 1640 channel. All future Cimel sun photometer units procured by NEON will be instrumented with the 1640 nm channel). Measurements were made on September 1st through 4th. One goal of the measurement is to use the derived atmospheric information to improve the atmospheric correction of the AVIRIS spectrometer data, in this case, the morning AVIRIS flight over OSBS on September 4, 2010. The sun photometer was not deployed on September 6 or 10 for the Donaldson Plantation flight or the OSBS mid-day flight.

Direct solar irradiance measurements from a well-calibrated radiometer can provide total optical depth that can be broken out into separate components as follows:

$$\delta_{\text{total}}(\lambda) = \delta_{\text{Rayleigh}}(\lambda) + \delta_{\text{aerosol}}(\lambda) + \delta_{\text{absorption}}(\lambda) \quad (1)$$

The Rayleigh component, also known as molecular scattering, is accurately predicted with known of atmospheric pressure[8]. The remaining aerosol and absorption components are subsequently derived in the Cimel processing[9]. Spectral aerosol optical thickness measured by the Cimel sun photometer on September 2, 2010 is shown in Figure 24. In order to characterize aerosol effect across the full spectrum, a power law[10] is assumed with a functional form:

$$\delta_{\text{aerosol}}(\lambda) = \delta_{\text{aerosol}}(\lambda_o)\left(\frac{\lambda}{\lambda_o}\right)^{-\alpha} \tag{2}$$

where α is the Ångstöm exponent and $\delta_{\text{aerosol}}(\lambda)$ is the aerosol optical depth at reference wavelength λ_0. The aerosol optical depth model based on the derived Ångstöm exponent for the Landsat 5 TM overpass at 15:51 UTC on 2 September 2010 is shown in Figure 25 with the associated experimental values from the Cimel sun photometer. The Ångstöm exponent corresponding to each of the aerosol optical depth measurements in Figure 24 is shown in Figure 26. These data are available from the NEON prototype data sharing site (http://neoninc.org/pds/).

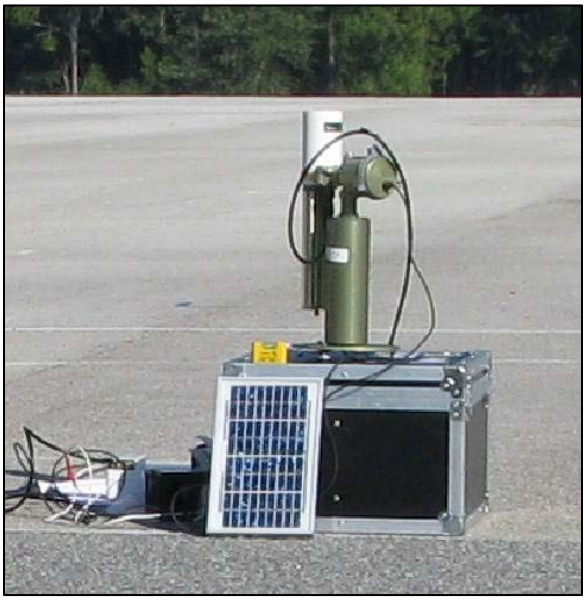

Figure 23. Cimel sun photometer show at the Driving Pad near the Gainesville Regional Airport

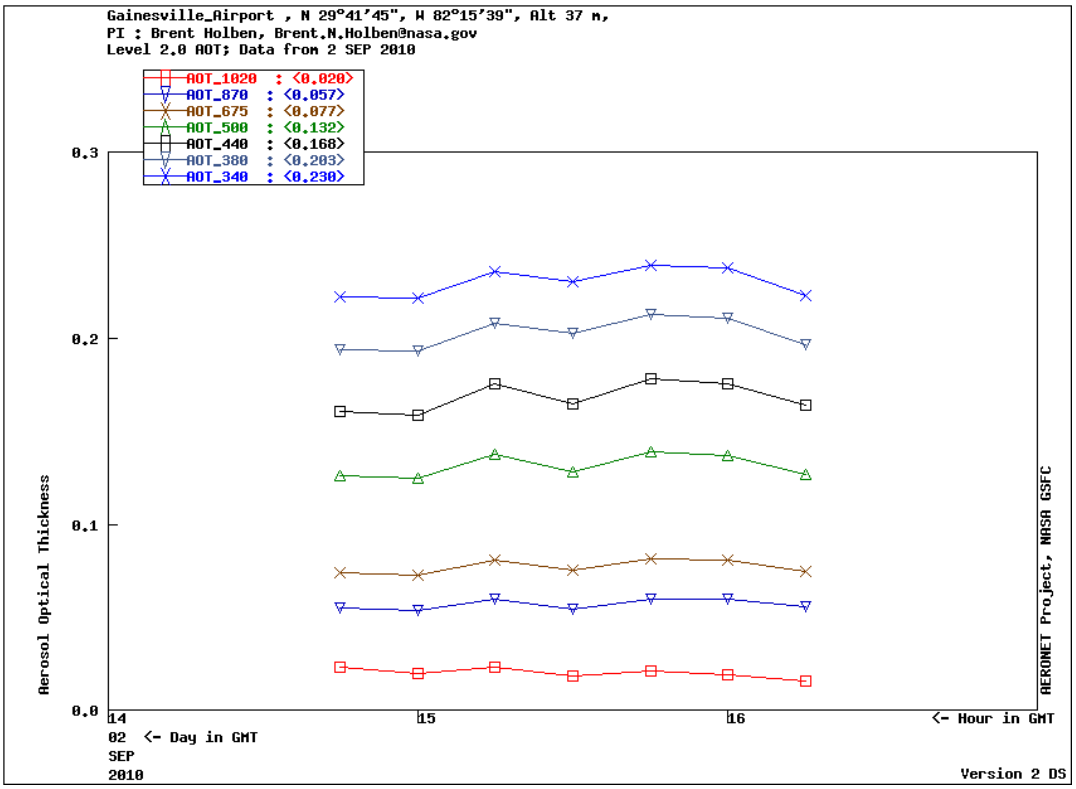

Figure 24. Aerosol optical thickness calculated from measurements with the Cimel sun photometer at the Driving Range on September 2, 2010

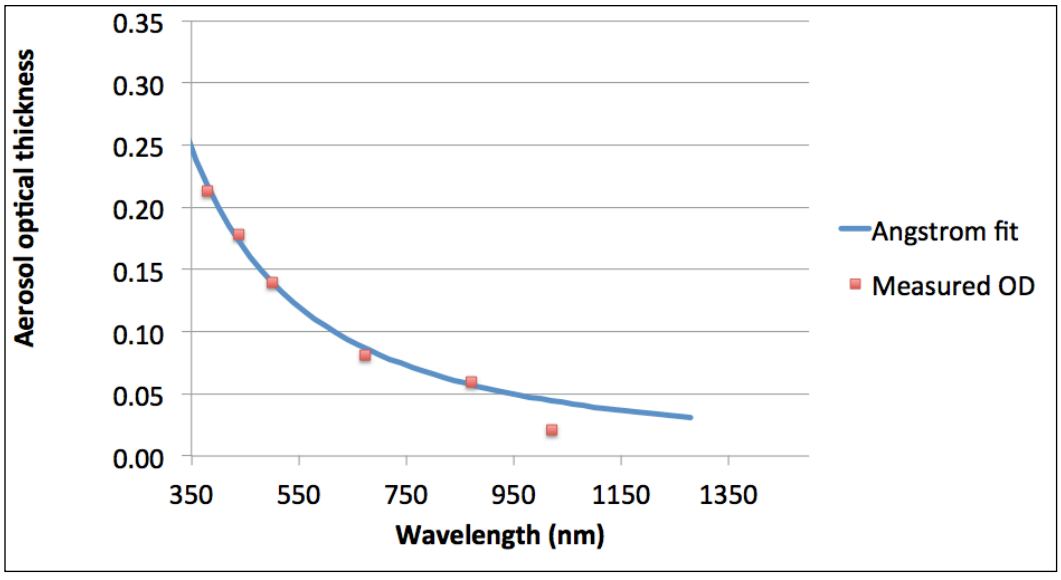

Figure 25. Aerosol optical thickness values derived from Cimel measurements for September 2, 2010 show good agreement with the Angstrom exponent fit derived from the Landsat 5 TM overpass at 15:51 UTC on September 2, 2010.

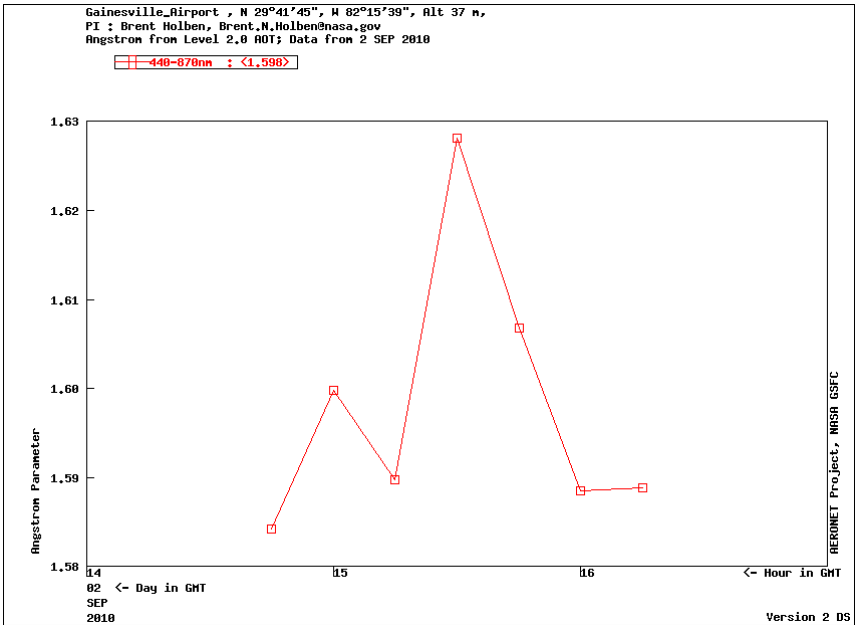

Figure 26. The derived Angstrom exponent for each of the aerosol optical depth measurements shown in Figure 24 over the course of the day on September 2, 2010.

Atmospheric water vapor will have a significant impact on the atmospheric transmission spectra. This can be seen in the modeled atmospheric transmission spectra with the water vapor component highlighted as shown in Figure 27. Column water vapor is calculated from the 940 nm spectral channel of the sun photometer[9]. Results for September 2, 2010 are shown in Figure 28.

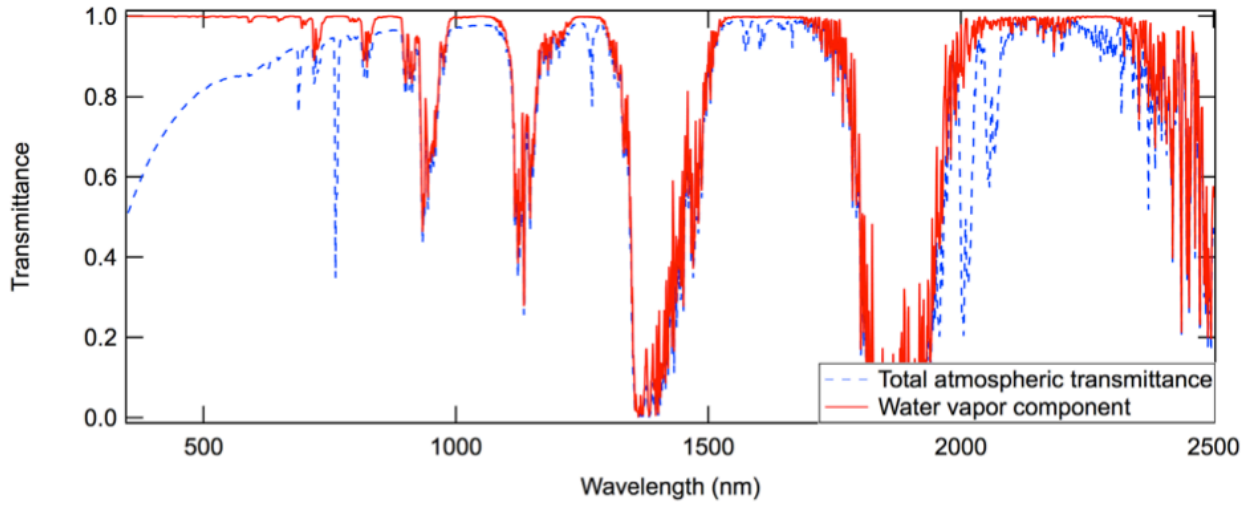

Figure 27. Total atmospheric transmittance also showing the component due to water vapor absorption

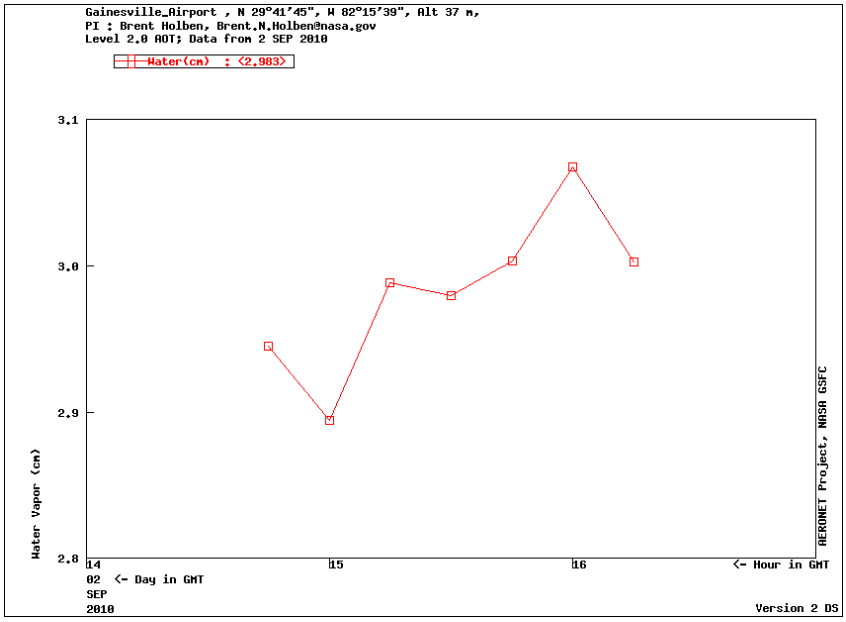

Figure 28. Column water vapor as measured on September 2, 2010

A Kestrel 4500 Pocket Weather Tracker portable weather station was used to collect temperature, pressure, relative humidity, and wind speed and direction. Measurements were made on August 31, September 1 through 4.

These measurements are used to assist in a correction on the GPS data collected within the aircraft during the research flight over OSBS on August 31 by NCALM. The three NEON base station measurements and the CORS data are used to determine the actual need for additional GPS base stations during NEON operations. Trimble R5 GPS base stations were used to measure highly accurate latitude, longitude and altitude measurements at three locations selected to augment the two NOAA CORS sites within the region.

6.2 Vicarious Calibration Experiment

A vicarious calibration experiment was implemented at a parking lot at the Gainesville Regional Airport that we called the *Driving Pad*. This test was conducted in order to help understand how the imaging spectrometer data would be affected in a humid environment and to further develop NEON protocols for this instrument validation effort. The calibration target used was an aged asphalt parking lot, having a high, flat and nearly Lambertian spectral reflectance, a large geographic size relative to the sensor pixel ground sample distance, therefore resulting in high spatial uniformity. This, coupled with a historic understanding of the site, and accessibility made this a good candidate for a calibration site. The atmospheric condition that existed during the flight campaign was low aerosol loading. Vicarious radiometric calibration utilizing ground truth measurements is how NEON will independently validate the laboratory radiometric calibration of the NEON airborne

spectrometer. The method used—called the reflectance-based approach—is very well studied and has been implemented on numerous spaceborne and airborne sensors[11,12]. The main purpose of the vicarious method is to determine the relationship between incident spectral radiance and the sensor output for the airborne spectrometer. This calibration is independent of on-board calibrators and pre-flight calibration and gives a perfect situation for cross-calibration with satellite sensors and other airborne spectrometers. Biases between sensors can be identified and removed.

The reflectance-based approach uses ground-based measurements of test site conditions in order to predict the radiance at the sensor. Ground measurements consist of surface reflectance of the test site and atmospheric conditions surrounding the test site. These measurements were collected on September 2 and 3 at the Driving Pad and on September 4 at OSBS during the pathfinder campaign. An ASD FieldSpec 3 Spectroradiometer, CIMEL sun photometer and Kestrel weather station were used to collect the data. In general, characteristics derived from these measurements are input to a radiative transfer code that predicts the radiance incident at the sensor and therefore gives a check on the coefficients derived in the laboratory to determine the radiance output of the sensor. During this experiment we aimed to utilize the well-known calibrations of AVIRIS and Landsat TM+ to check our field approach and methodologies.

Measurements of test sites are alternated with measurements of the field reference panel. These measurements allow the test site to be referenced to the field reference panel. A schematic of the measurement sequence is shown in Figure 29. Reference measurements (white boxes) are taken before and after each round-trip transect measurement (blue arrows).

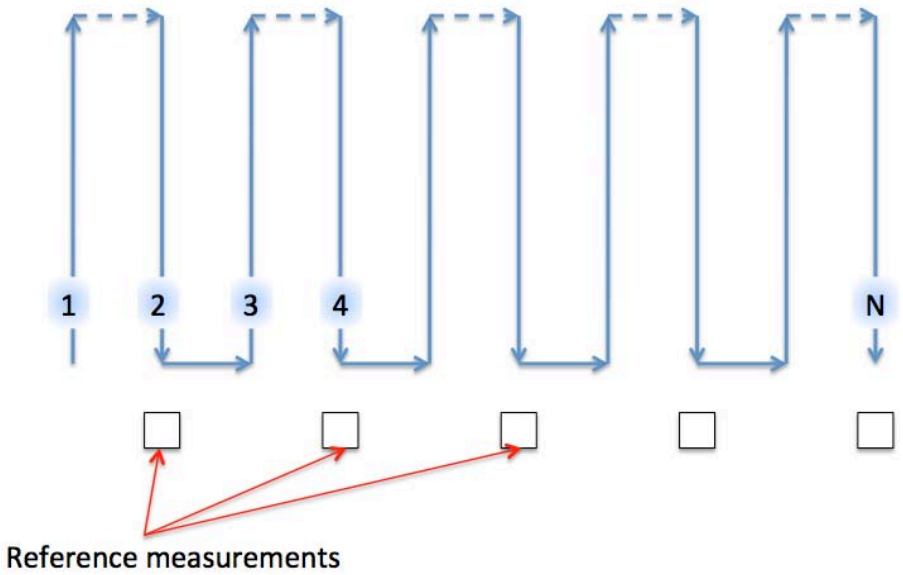

Figure 29. Transect measurements with alternating reference measurements

The length, separation and number of transects used for a test site depend on the sensor being characterized and the size of the test site. For example, a Landsat-type sensor with 30 m GSD might have 60-120 m long transects with 15-20 m separation and an AVIRIS-type sensor with 4 m GSD

might have 32-40 m long transects with 4-8 m separation. The number of transects will depend on the test site and measurement completion in a reasonable amount of time. Exact test site designs used during the Pathfinder mission is shown in Table 5. Figure 30 shows a NEON team member carrying an ASD spectroradiometer along a transect of the 60 × 180 m Landsat site. He will complete the current transect, measure the white reference panel and continue measurements of the following transect.

Table 5. Pathfinder test site designs

	Landsat site	AVIRIS asphalt	AVIRIS vegetated
Location	GNV asphalt lot	GNV asphalt lot	Ordway-Swisher
Transect length	60 m	40 m	32 m
Transect separation	20 m	8 m	4 m
Number of transects	10	13	11
Dimension	60 × 180 m	40 × 90 m	32 × 40 m
Measurement time	15 min	9 min	14 min

Figure 30. Surface reflectance measurements of the aged asphalt site

Following the calculation of the site bidirectional reflectance factor (BRF) and accounting for the reference panel BRF, the site reflectance values were determined. Figures 31-33 show the reflectance of each test site in the black solid line and percent standard deviation in the dashed red line. Standard deviation gives a good indication of site variability. These plots show that the 48% tarp has the highest uniformity where the vegetated site has the least. Despite the 48% tarp being the most uniform, the aged asphalt is the most ideal test site used during the Pathfinder mission due to its large size, brightness and uniformity.

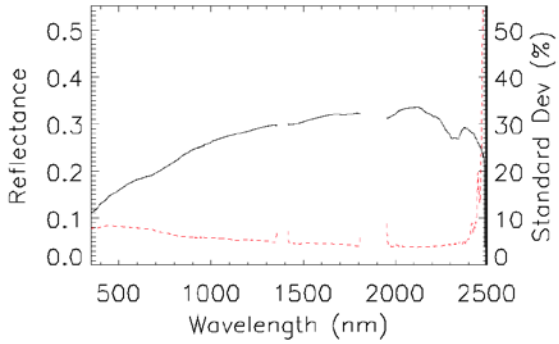

Figure 31. Aged asphalt reflectance.

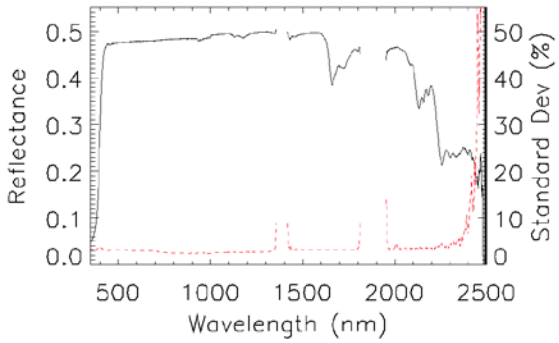

Figure 32. 48% tarp reflectance.

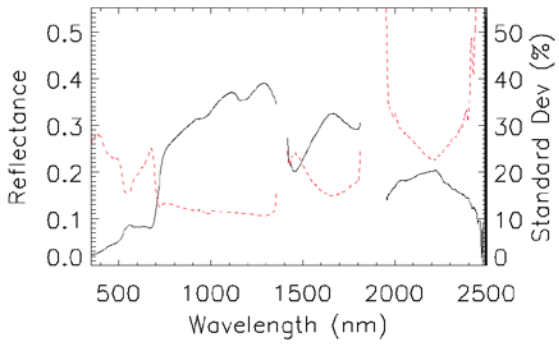

Figure 33. Vegetated site reflectance

6.3 Radiative transfer

The surface and atmospheric properties determined above were used to constrain radiative transfer code that predicts at-sensor radiance for airborne and space-based imagers. The code accounts for user-defined atmospheric and surface conditions and calculates the corresponding components of at-sensors radiance including directly reflected radiance, atmospherically diffuse reflected radiance, and upwelling atmospherically scattered radiance. These components have significant spectral

dependence. Most of the spectrum is dominated by the directly reflected component of at-sensor radiance with portions of heavy absorption due to water vapor. The blue end of the spectrum becomes more sensitive and is ultimately dominated by Rayleigh and aerosol scattering.

The radiative transfer code assumes a solar spectrum and simulates its path through the atmosphere to the ground, its interaction with the ground, and finally its path towards the sensor. The code used in this work is MODTRAN®[13,14]. MODTRAN® approximates the atmosphere and Earth's surface as a sequence of layers. Each layer has its own transmission and scattering contributions to the total radiance. The bottom layer is Earth's surface and is modeled to be opaque and characterized by the input reflectance spectrum. Transmittance calculations are based on band models of molecular line absorption, continuous molecular absorption, and extinction coefficients of aerosols.

Radiance values obtained from the airborne or space-based imager corresponding to the test site are compared with predicted values that are band-averaged from the output of radiative transfer code[15]. Results in this section are presented as percent difference following

$$\%\ \text{difference} = 100 \cdot \frac{L_{\text{sensor}} - L_{\text{NEON}}}{L_{\text{sensor}}} \tag{3}$$

where L_{sensor} is the radiance reported by the sensor and L_{NEON} is the predicted at-sensor radiance. Figure 34 shows results for the Landsat 5 TM acquisition of the aged asphalt test site on September 2, 2010. There are two sets of results named "Regular" and "Adjacency" that vary significantly, especially in the first three bands. The "Regular" data set uses only the test site reflectance meaning that the radiative transfer code assumes that the entire surface has that spectral reflectance. This becomes a problem if the surface surrounding the test site has drastically different reflectance, which is the case for the aged asphalt and 48% tarp. The problem arises from atmospheric scattering and effects the atmospherically diffuse reflected radiance and upwelling atmospherically scattered radiance components of total at-sensor radiance. MODTRAN has the option to specify the surrounding reflectance to account for this and these results are shown in Figure 34 as "Adjacency." The largest differences appear in the visible portion of the spectrum due to the combined effects of drastically different reflectance and increasing atmospheric interaction towards shorter wavelengths.

Figure 35 shows results of these comparisons for AVIRIS using the test sites considered in the Pathfinder mission. MODTRAN inputs for the aged asphalt and 48% tarp include a vegetation reflectance input for the "adjacent" reflectance. The four sets of results lie about ±10% from each throughout most of the spectrum. Inspecting the shape of each of the lines shows that all four sets of results share similar band-to-band features even though the reflectance spectra of the test sites are significantly different. This gives confidence in the results despite large offsets from each other.

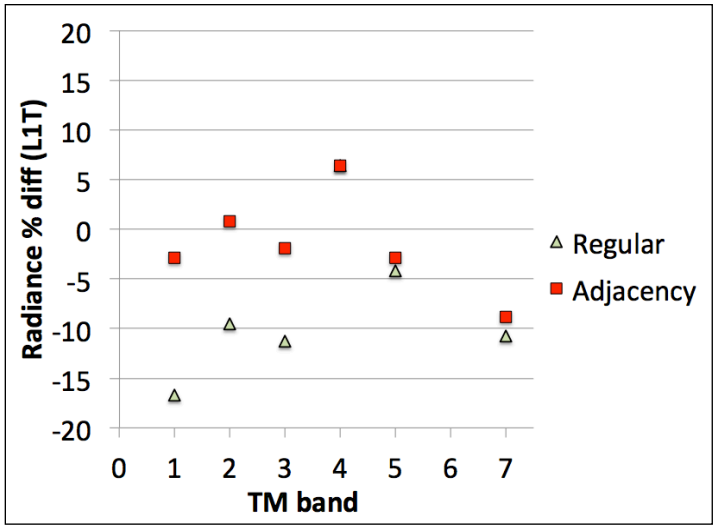

Figure 34. At-sensor radiance comparisons for Landsat 5 TM on 2 September 2010

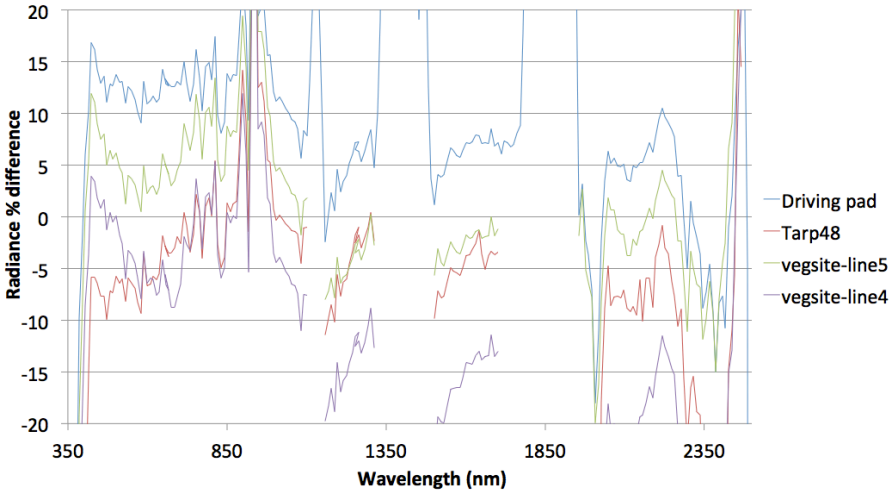

Figure 35. At-sensor radiance comparisons for AVIRIS

6.4 Airborne and ground reflectance retrieval comparisons

Ground spectral measurements of individual vegetation species can help to inform interpretation of information retrieved by the airborne spectrometer over a sample region containing those species. It can be helpful to take the measurements from above the canopy tops so they are similar to the measurements taken by the airborne spectrometer in that the leaves are in a similar orientation to the aircraft retrieval and the surrounding environment and ground is included in the measurement. During this campaign, measurements were made both from the ground and from an aerial boom lift

(Fig. 36). An ASD FieldSpec 3 Spectroradiometer was deployed out at OSBS to make spectral reflectance measurements of several vegetation species over the 400-2500 nm wavelength range on August 31 and September 1. Measurements of reflectance of several species including Pindo Palm, short wiregrass, and fennel were collected from the ground. An aerial boom lift was employed to measure the canopy top reflectance of the Longleaf Pine, Sand live oak, Turkey Oak, and mixtures of the spectral signatures of turkey oak and longleaf pine as shown in Figures 37-40. GPS coordinates were recorded for each reflectance measurement in order to help locate the plants in the AVIRIS imagery.

Figure 36. Above-canopy spectroscopic measurements at OSBS using the ASD FieldSpec instrument from atop an aerial boom.

The spectral shapes of the AVIRIS and ground-based reflectance shown in these figures exhibit similarities but their brightness show much disagreement. The reasons for this inconsistency include different view angles in the measurement techniques and the smaller footprint size of the ground-based measurements. The most agreement between ground-based and AVIRIS-derived reflectance is seen from the Long leaf pine and Turkey oak combination shown in Figure 40. This approximately 20 m × 20 m scene contained about equal canopy areas of the two tree species. The ground-based measurement was made by sweeping the scene by hand and thereby provided an average spectral reflectance for the area. The AVIRIS-derived spectral reflectance was derived by averaging several pixels (~30) from the imagery. The better agreement seen here relative to point-based comparisons

could be attributed to similar spectral mixing by sweeping the ground measurements thereby capturing a similar spectrum as the 4 m AVIRIS pixels, and higher AVIRIS signal due to averaging.

The airborne and ground-based reflectance retrieval is also compared for the 48% tarpaulin as shown in Figure 41. Just as the single pixel comparisons for the dominant tree species, there is significant noise in the AVIRIS-derived reflectance. There is considerable agreement despite the small size of the tarpaulin (10 m square) relative to an AVIRIS pixel (~3.6 m square).

Comparisons such as these will continue in an effort to develop confidence in current and new atmospheric compensation algorithms. Future work will put more emphasis on viewing geometries and may go as far to characterize several view and illumination geometries[15]. Such measurements and studies are important because of the NIS's wide field-of-view (± 17°) and long acquisition time (2-4 hours).

In Figures 37-41, the red line corresponds to airborne measurements from AVIRIS and the black line corresponds to the ground measurement.

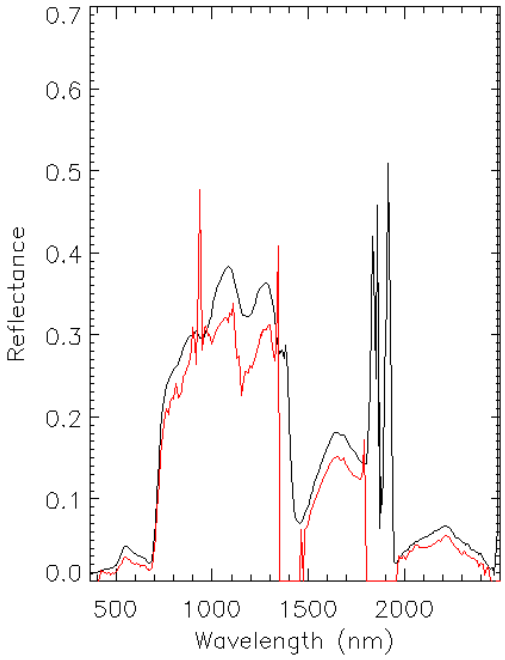

Figure 37. Turkey Oak (*Quercus laevis*) reflectance.

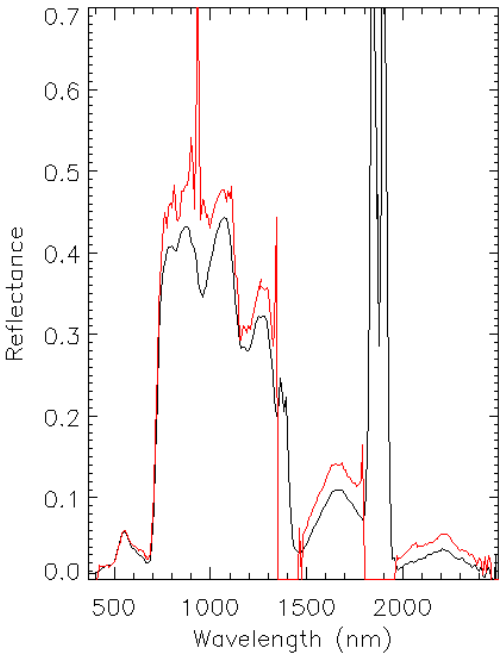

Figure 38. Long-leaf Pine (*Pinus palustris*) reflectance. The drop-off in AVIRIS reflectance near 980 and 1300 nm is due to strong water vapor absorption bands in the atmosphere.

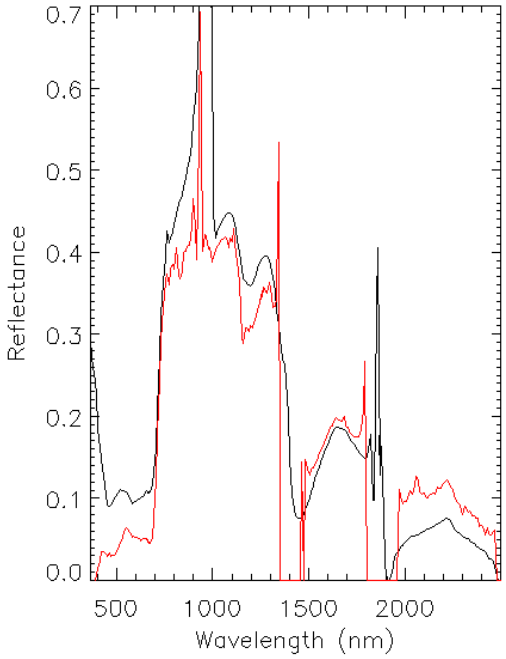

Figure 39. Sand live oak reflectance.

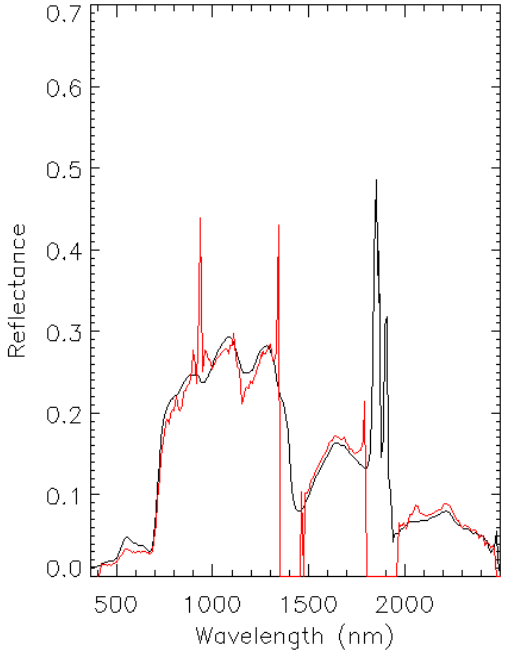

Figure 40. Turkey oak and Long-leaf pine mix reflectance.

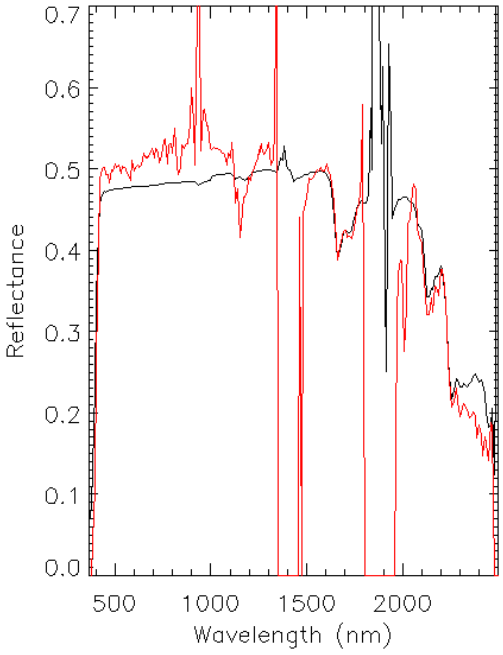

Figure 41. 48% tarp reflectance.

Spectral datasets for individual plant species have been generated and have been made available to the public via the NEON web portal (http://neoninc.org/pds/). Two files are provided for each spectral reflectance dataset, a jpeg image and an ASCII text file. The jpeg shows a preview of the data including a description of the object being measured, information about the date and time of the collection, the GPS coordinates of the object, a photograph to provide context about the object, and a quick look of the reflectance spectrum and standard deviation of the measurement. The text file contains the reflectance measurement data as 3 columns: wavelength (nm), reflectance (mean of several measurements), standard deviation of the measurement. Measurements of the canopy top reflectance of the Longleaf Pine, Turkey Oak, and a mixture of the spectral signatures of both types of trees along with ground reflectance measurements of a Pindo Palm, short wire grass, and fennel are provided. An example jpeg image from a Longleaf Pine measurement is shown in Figure 42.

6.5 Satellite overpasses

Several NASA satellites acquired imagery over Florida around the time of the Pathfinder Campaign. In the case of EO-1 Hyperion and ALI, the EO-1 instruments were actively tasked to collect imagery over OSBS and Gainesville, FL. Other instruments such as Landsat-5 TM, Landsat-7 ETM+, and Terra/Aqua MODIS collect imagery over land as part of their routine science operations. A list of satellite overpasses containing imagery of OSBS, Donaldson Plantation, and surrounding areas is given in Table 1.

Table 6. List of satellite overpasses concurrent to the NEON pathfinder campaign.

Date		Sensor	Cloud Cover
YYYY-MM-DD	YYYY-DDD		
2010-08-01	2010-213	TM	Partially cloudy
2010-08-02	2010-214	ETM+	Partially cloudy
2010-08-09	2010-221	ETM+	Partially cloudy
2010-08-10	2010-222	TM	Cloudy
2010-08-17	2010-229	TM	Partially cloudy
2010-08-18	2010-230	ETM+	Clear
2010-08-18	2010-230	Hyperion	Clear
2010-08-18	2010-230	ALI	Clear
2010-08-25	2010-237	ETM+	Partially cloudy
2010-08-26	2010-238	TM	Cloudy
2010-09-02	2010-245	TM	Possible cirrus
2010-09-03	2010-246	ETM+	Clear
2010-09-03	2010-246	Hyperion	Clear
2010-09-03	2010-246	ALI	Clear

```
Site:                 D03_core                    Field notes: above canopy long leaf pine.  3285188.6, 403313.6
Date measured:        2010 Aug 31                 Samples selected:  005-009  18:28:08
Date processed:       2011 Mar 14
First sample time:    18:28:05 UTC
Last sample time:     18:28:11 UTC
Solar position start: 25.44 zen, 216.50 azi
Solar position end:   25.45 zen, 216.55 azi
lat/lon:              29.698, -81.988

Directory of reference data: /neon/data/aop/panel/aops1/factory/
Directory of spectra:        /neon/data/aop/field/D03_core/100831/refl/os_pos2/
Directory of processed data: /neon/data/aop/field/D03_core/100831/refl/os_pos2_processed/
```

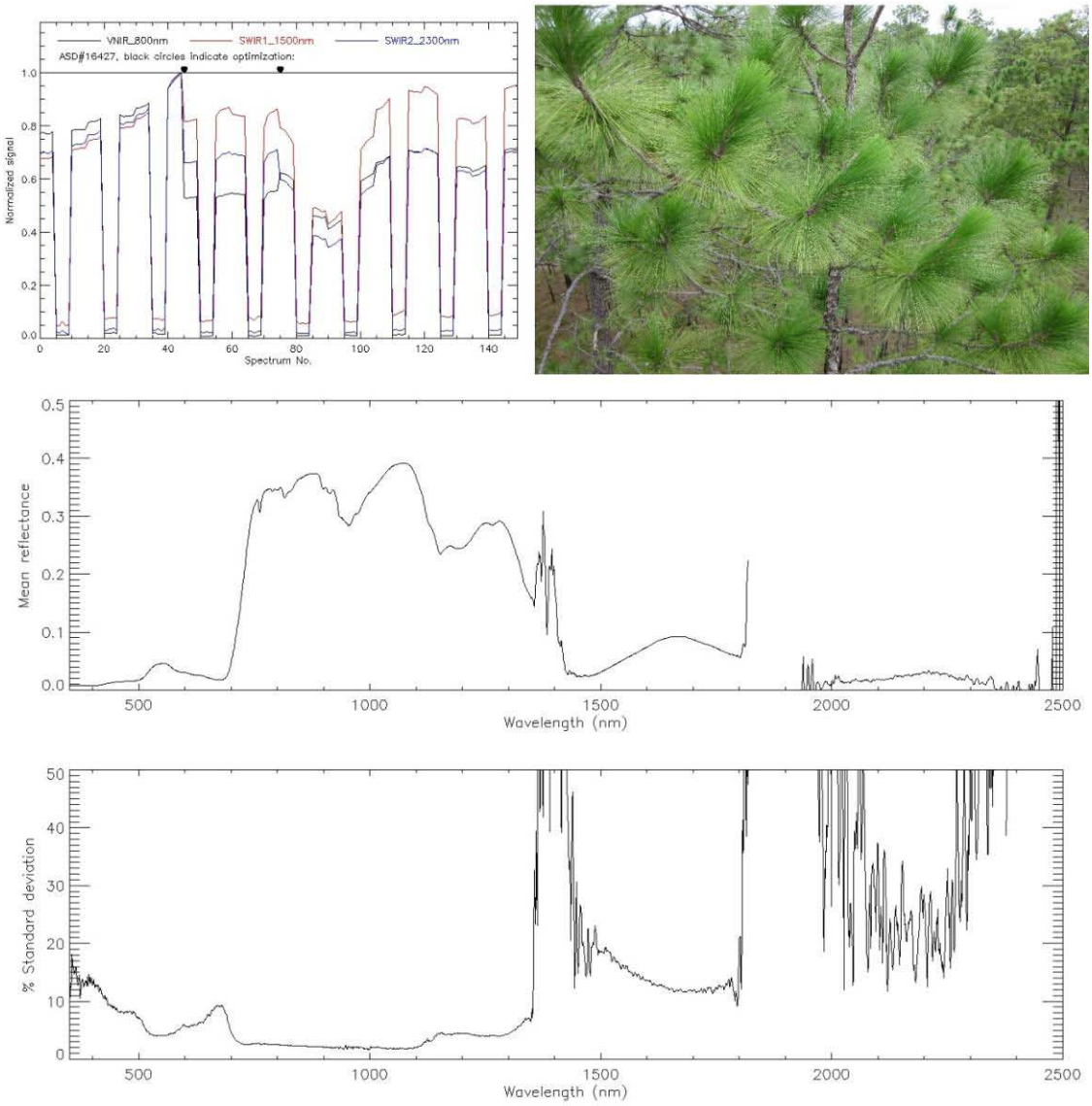

Figure 37. JPEG quick view of a reflectance measurement of Longleaf Pine

7 PRELIMINARY SCIENCE RESULTS

7.1 Field sampling results

The following sections contain results from the field sampling portion of the work focused on leaf area index (LAI), vegetation structure, plant biodiversity plot design, and invasive species monitoring. Specifically, we analyze how the data that were collected on the ground address the seven goals stated in Section 5 of this document.

7.1.1 Protocol and training development

Protocols for plot and transect delineation, measurement of LAI and vegetation structure, plant biodiversity monitoring, and identification and mapping of an invasive species were generated by NEON staff. A combination of classroom and field instruction was employed to train field crew members, and questionnaires given to field crew members allowed NEON staff to determine where improvements in hiring, training, and data collection could be made. Experiences with the equipment used to measure LAI and vegetation structure in Florida have lead directly to a series of prototype efforts to optimize the equipment and workflow used to obtain these data.

7.1.2 Collection of ground validation datasets

An important initial goal for the 2010 Florida field work was to obtain ground datasets that could be used to validate both the airborne hyperspectral and LIDAR instruments. As such, we chose to measure both LAI (to validate maps of LAI generated from either the hyperspectral or LIDAR instruments), and a suite of vegetation structure variables from individually geo-referenced trees and shrubs. Vegetation structure measurements included: height, height to first branch, canopy diameter, diameter at breast height, species ID, and whether an individual was alive, dead, horizontal, etc. More details about these two datasets are provided in the two sections below.

7.1.3 Leaf area index validation results

At the OSBS site, LAI was measured along eight 500 m length transects located in the Sandhill vegetation type that dominates the proposed NEON tower footprint. Sandhill vegetation is characterized by a semi-open canopy dominated by Long-leaf Pine (*Pinus palustris*) and Turkey Oak (*Quercus laevis*). LAI was measured along six similar 500 m length transects at the Donaldson Tract, which is an even-aged Slash Pine (*Pinus elliottii*) plantation. At both sites, we compared two instruments for measurement of LAI: the LICOR LAI-2200 plant canopy analyzer, and an off-the-shelf digital hemispherical photo (DHP) system comprised of a Nikon D300 DSLR body, a 10.5 mm Nikkor fish-eye lens, and a GP-1 GPS receiver. The camera was mounted on a monopod, and bubble-levels were attached to the monopod to ensure that the DHP system was as close to perpendicular to the ground as possible when images were taken. For the DHP system, both upward and downward-facing photos were taken every 50 m along three 500 m length transects: one transect at OSBS, and two transects at the Donaldson Tract. Nikon View NX software was used to perform initial image QA/QC, and Can-Eye software was used to analyze selected DHP images and calculate LAI.

Because upward and downward-facing images were collected with the DHP system and only canopy LAI was measured with the LAI-2200, we compared data acquired via these two methods with LAI

estimates derived from airborne remote sensing instruments in order to determine whether understory plants contributed significantly to remotely-sensed LAI. At the Donaldson Tract, we found that the distribution of LAI values derived from airborne remote sensing was centered on an LAI value that was significantly higher than the distribution derived from the LAI-2200 instrument. This result is likely explained by the fact that although the Slash Pine plantation canopy was relatively homogeneous in terms of canopy cover, there was considerable Saw Palmetto (*Serenoa repens*) understory cover that the LAI-2200 did not account for due to the fact that the instrument was held 2 m aboveground during data logging (Figure 38).

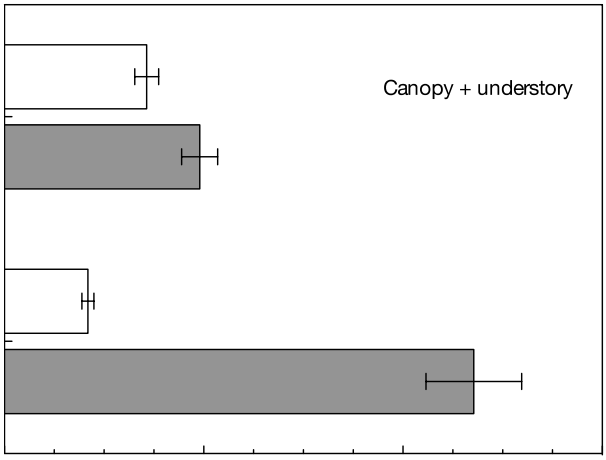

Figure 38. Leaf area index at the Donaldson Tract Slash Pine plantation, showing variable effects of understory vegetation on ground-based estimates of LAI.

At OSBS, the remote-sensing LAI distribution derived from the entire site (roughly 20 km^2) showed a greater number of low LAI values and a longer right-tail than the ground-measured LAI distribution from the Sandhill ecosystem (Figure 39).

We attributed the greater number of low values in the remotely-sensed LAI distribution to the fact that the airborne remote-sensing instrument has a higher spatial resolution than the LAI-2200, increasing the chances that low values will be recorded from gaps in the canopy with sparse ground vegetation cover. The larger spatial footprint of the LAI-2200 means that gaps would be averaged with areas containing trees, thus shifting the left tail of the distribution toward the center. The long right-tail of the remotely-sensed LAI distribution was likely not captured with the LAI-2200 due to two reasons: 1) ground sampling was restricted to the Sandhill ecosystem, which has relatively low LAI compared to some of the less dominant forest types captured by the airborne instrument across the site; and 2) as already mentioned, the LAI-2200 averaged pixels with very high LAI values with lower LAI pixels, due to the coarser resolution of the sensor compared to the airborne sensor, thus compressing the right-tail of the distribution toward the center.

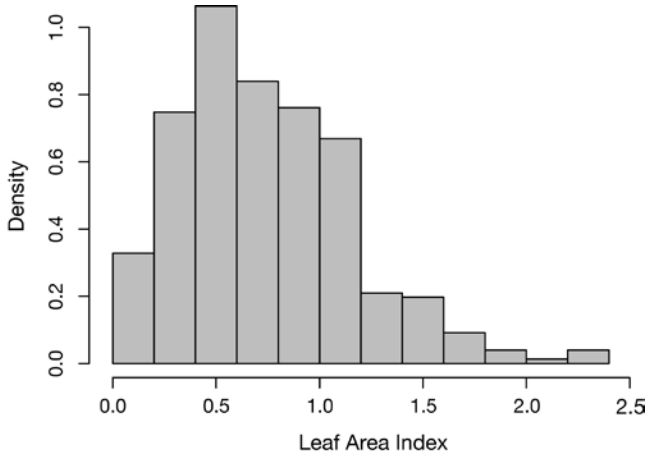

Figure 39. Density distribution of LAI values at OSBS, measured along eight 500 m length transects with a LICOR LAI-2200.

Summary: Although we could not obtain finer resolution LAI estimates from the ground, due to the nature of commercially available equipment, it is clear that ground-collected LAI validation datasets must be sampled across the site, rather than sampling from only the dominant vegetation type (Sandhill in this case). This strategy will allow a greater range of LAI values to be sampled, and will better reflect the distribution of LAI observed via the remote-sensing instruments. Furthermore, at both sites, we initially assumed that canopy trees would account for the majority of the LAI observed via the remote sensing instruments, and therefore a protocol that maintained the LAI-2200 sensor at 2 m aboveground would be appropriate for obtaining useful field validation data. However, these results clearly show that field methods for estimating LAI and validating remotely-sensed datasets must account for the understory vegetation component.

7.1.4 Vegetation structure validation results

At OSBS, vegetation structure data were collected from a 20 m × 120 m plot that overlapped the northernmost of the tower footprint transects (Figure 40 and Figure 41). As part of this effort, data were collected from 286 live and dead individual trees and shrubs ≥ 1 m in height.

Several months prior to the NEON vegetation structure ground sampling effort, the vegetation was burned as part of routine site management. Dead small-stature oaks resulted from the burn, which are evident in Figure 41 as small bunches of dead leaves ~ 1 m off the ground, with a flush of green leaves emerging at ground level. The mapped locations of dead, small-stature Turkey Oaks resulting from burn management are shown in Figure 42. Analysis of these data showed that the LIDAR instrument did not detect these small, dead individuals. As such, it is not possible to detect the effects of fire management using a single LIDAR snapshot in this ecosystem.

Figure 40. Aerial image of the vegetation structure plot at the OSBS site. Red points indicate the location of high-resolution GPS measurements.

Figure 41. Field crew collecting vegetation structure data at OSBS.

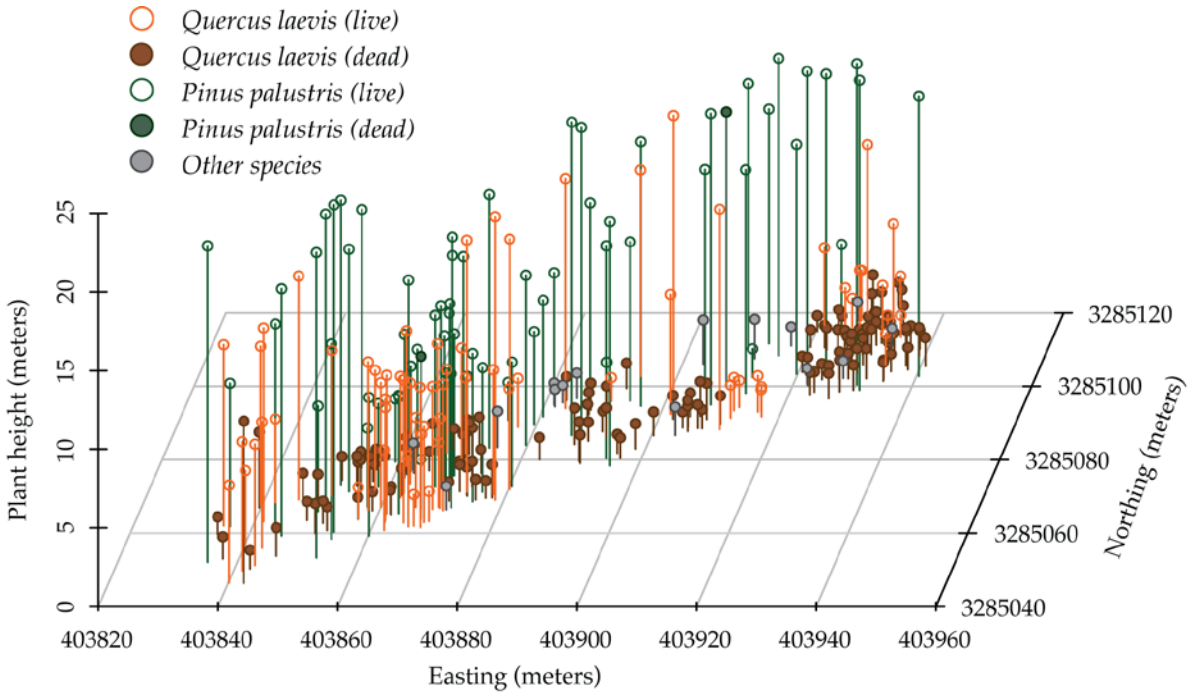

Figure 42. Location and height for all plants ≥ 1 m height, and rooted within the vegetation structure plot at the OSBS site.

The shortest vegetation mapped included trees and shrubs equal to 1 m height, and the tallest tree mapped was a Long-leaf Pine that was 20.8 m in height. Because Long-leaf Pines are among the tallest trees at OSBS, ground-based height measurements spanned a similar range of variability as the remote-sensing LIDAR measurements, and these measurements therefore formed a viable ground-validation dataset.

We also measured minimum and maximum canopy diameter, as well as height to first branch from the ground in order to obtain a reference point for canopy delineation within the airborne LIDAR dataset. Minimum and maximum canopy diameters were estimated visually from the ground using meter tapes, and average canopy diameter was calculated via the geometric mean (Figure 43; in the figure, the circular "X" symbols represent plot markers with high-resolution GPS coordinates).

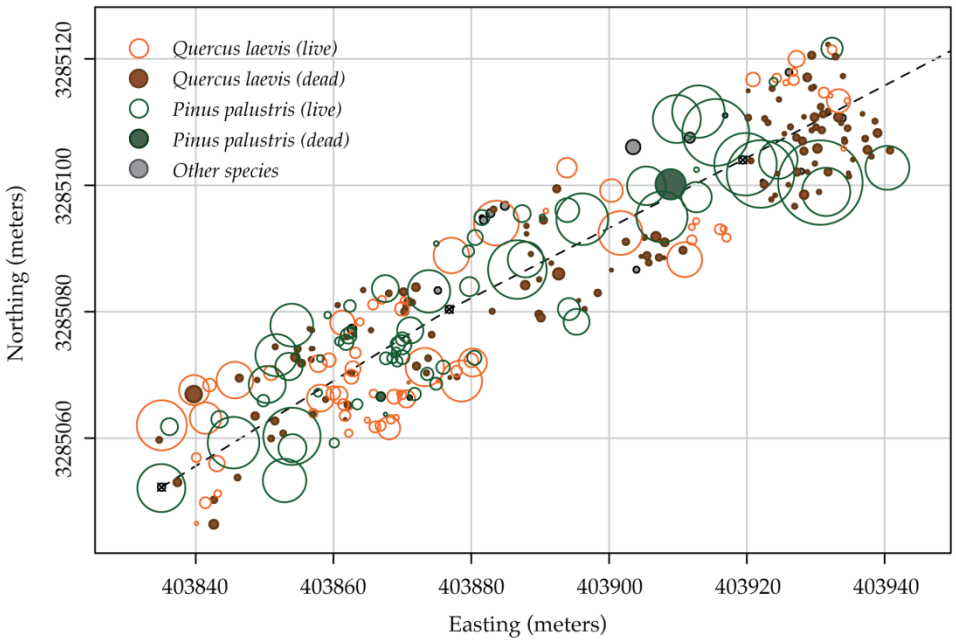

Figure 43. Location and average canopy diameter in meters for all individuals ≥ 1 m in height rooted within the vegetation structure plot.

7.1.5 Implications for ground validation strategy

The LAI and vegetation structure results presented here are instructive with respect to developing a sound ground validation strategy for airborne remote sensing datasets across the NEON sites. For LAI, it is clear that methods for obtaining validation datasets must account for contributions from understory vegetation, and measurement locations must be chosen such that the full range of variability in LAI is recorded. For this work, LAI was only recorded from a Sandhill ecosystem at OSBS, resulting in a lack of ground data from high-LAI vegetation types (e.g. Xeric Hammock). As a consequence, we are confident that the algorithm employed to calculate LAI from the remote-sensing datasets produces distributions of values relatively close to those obtained from the ground for a Sandhill ecosystem, but it is not possible to validate the algorithm at levels of LAI greater than two.

For the vegetation structure validation dataset, selection of one 20 m × 120 m plot allowed the mapping, identification, and measurement of a sufficiently large number of trees and shrubs to validate height, canopy dimensions, and stem locations derived from the LIDAR dataset. We found that the 1 m height cut-off was appropriate given that it is difficult to differentiate individual plants less than 1 m in height from each other in the LIDAR datasets (data not shown). Given that the Sandhill ecosystem contains the tallest trees at OSBS, and the plot was large enough to contain numerous very tall, large-canopy trees (Figure 42 and Figure 43), the vegetation structure dataset spanned the same range of vegetation structure variability as the remote-sensing dataset, which is highly desirable. However, future vegetation structure ground validation efforts should focus on sampling from multiple plots distributed across the site of interest. This is because LIDAR and hyperspectral remote-sensing datasets may be used to identify individual stems to species – based on characteristic structural or spectral traits – and ground sampling should sample individuals growing

across the full range of site conditions in order to best discriminate among species. Differences in site conditions may cause the physical or chemical morphology of species to change, and a comprehensive ground-validation dataset must account for this potential intraspecific variation in morphology.

7.1.6 Timing of field sampling

One unknown with respect to calibrating remotely sensed airborne data with ground-collected data is the width of the temporal window in which collection of these two datasets must occur within a given ecosystem. To address this question, LAI data were collected at OSBS from the tower footprint transects (shown in yellow in Figure 19) at two different time points approximately 2 weeks apart. Field crews collected data during mid-August and at the beginning of September during the airborne flights. Analysis of these data show that LAI does not change significantly between these two time points when analyzed at the transect scale (ANOVA, $p<0.05$; Figure 44), and in general, LAI values at various positions along each transect were congruent with each other between the two measurement timepoints (e.g. Figure 45). These results indicate that for the OSBS site, ground and airborne data collection can likely occur within 2-4 weeks of each other. Results such as these are useful within the context of developing operational ground and flight logistics.

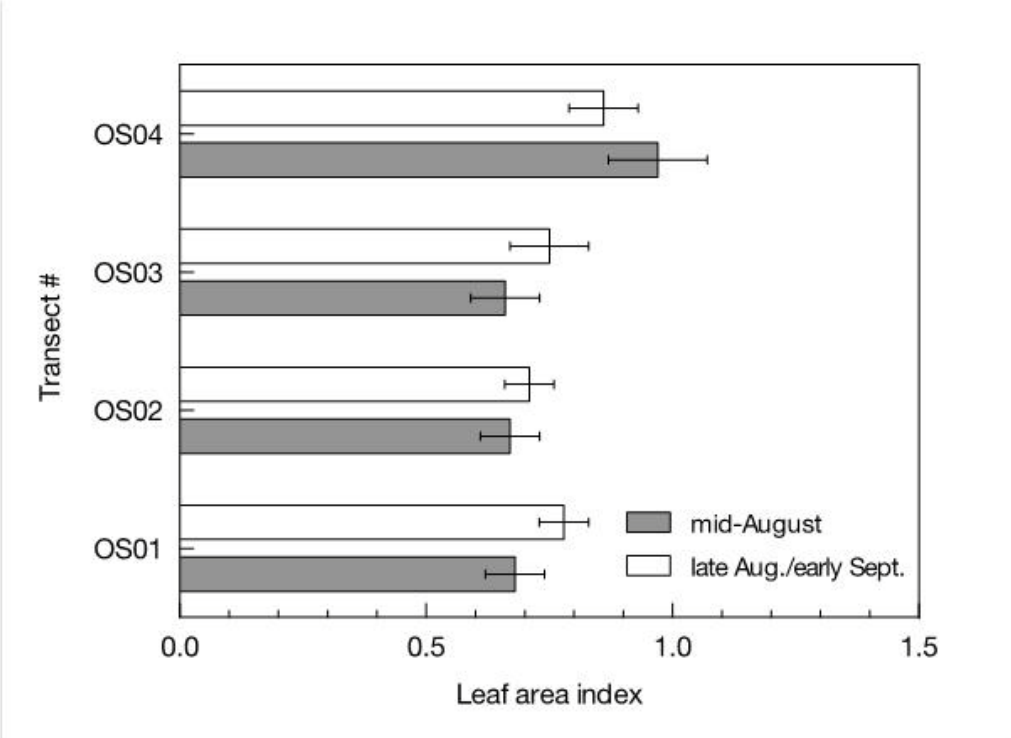

Figure 44. A comparison of LAI data collected approximately two weeks apart at the OSBS site. The transects shown here are depicted in yellow in Figure 19. Analysis of variance indicates LAI values are not different between mid-August and late August/early September.

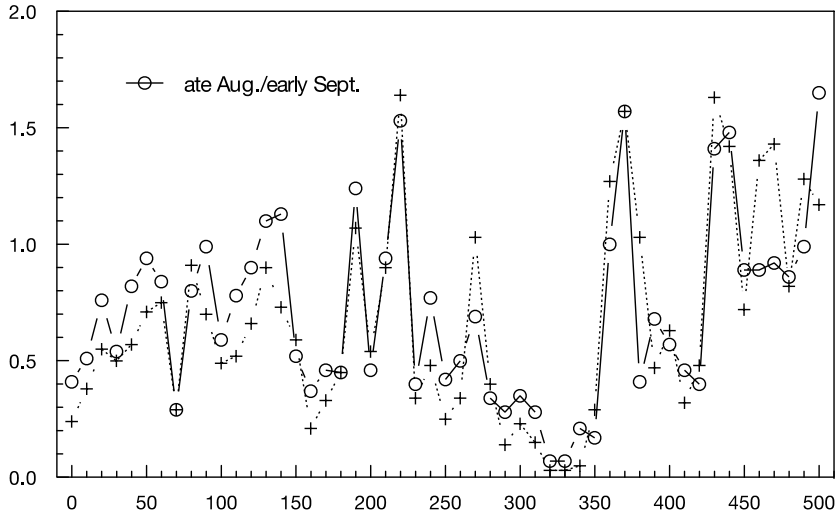

Figure 45. Leaf area index measured at two different timepoints along a transect in the tower footprint at OSBS.

7.1.7 Optimizing ground sampling design

In addition to validation of remote sensing datasets, one requirement for the NEON terrestrial plant sampling is to enable partitioning of net primary productivity into its major vegetation components within the tower footprint where eddy covariance measurements are also made. From a sampling design perspective, this requirement necessitates answering the following four questions: 1) how many elemental sampling units (ESUs) are needed? 2) what is the optimal ESU size? 3) what is the optimal ESU shape? and 4) how far apart should ESUs be spaced? We addressed questions 2 and 4 by analyzing LAI data collected from eight transects at OSBS located in Sandhill vegetation.

Sample number analysis

To address question 2 above, we performed a sample number analysis using LAI data collected with an LAI-2200 instrument every 10 m along eight 500 m length transects. Prior to the analysis, all data were screened to ensure that the signal:noise ratio was > 100, as per LICOR technical recommendations. Sample number (*n*) was estimated according to Equation 4:

$$n = \frac{t^2 \times CV^2}{AE^2} \quad (4)$$

where *t* is the student's t-statistic for the appropriate degrees of freedom (assumed that d.f. = ∞), *CV* is the coefficient of variation from the sample dataset (calculated as CV = sample standard deviation / sample mean), and *AE* is the level of acceptable error that is desired – e.g. a value of 0.2 indicates *n* is calculated such that the variable of interest will be estimated to within 20% of the population mean. Equation 4 assumes that the input data used to calculate *CV* are normally distributed, and in this case, LAI data were square-root transformed in order to meet this assumption (Figure 39 shows that the distribution of LAI values from the 8 sampled transects is not normally distributed). Using

Equation 4, we found that 26 data points are required to estimate LAI to within 10% of the mean and with 90% confidence ($\alpha/2 = 0.05$). We also calculated the *n* required to estimate LAI across a range of *AE* values, and with 70%, 80%, 90%, and 95% confidence (Figure 46).

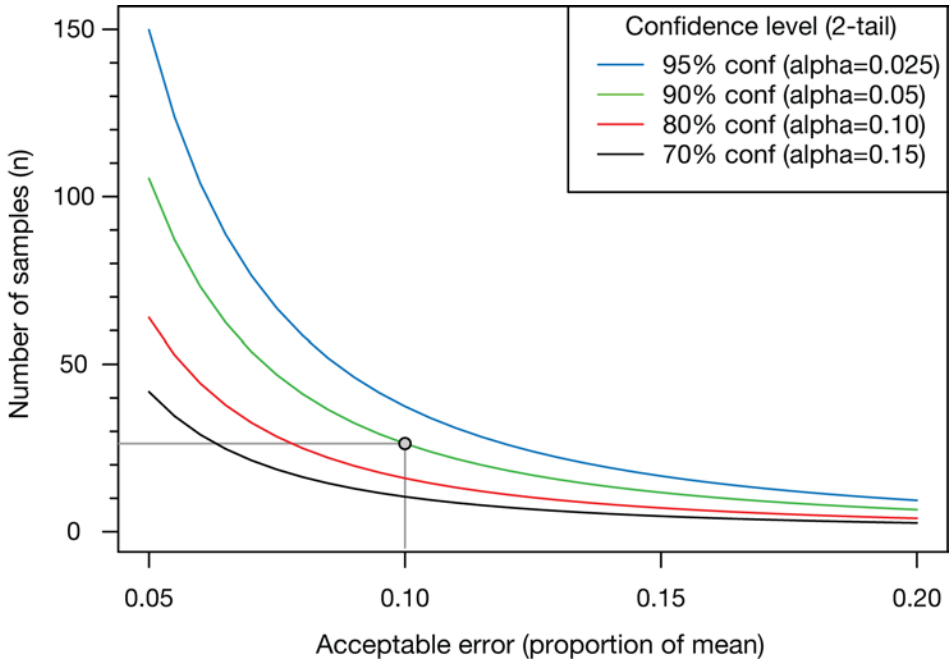

Figure 46. Sample number analysis based on Leaf Area Index data collected from Sandhill vegetation dominated by Long-leaf Pine and Turkey Oak.

Optimizing sample spacing

The degree to which vegetation is patchy at the landscape scale, the size of those patches, as well as what types of vegetation makes up patches are important factors that influence how far apart sampling locations should be. In a perfectly homogeneous landscape, ESUs can be close to each other or far apart, and the location of the ESUs will not influence the LAI estimate at the landscape scale. However, if vegetation is not distributed homogeneously across the landscape, an accurate estimate of LAI requires minimization of the degree of spatial autocorrelation among measurement locations, as well as sufficient sample size. Satisfying this requirement means that the data that are then collected are as spatially independent from each other as possible, and the field sampling effort produces the most information per unit time spent gathering data.

Because the LAI dataset we collected is spatially explicit, we performed a semivariogram analysis in order to determine the optimal distance that should separate ESUs. We hypothesized that the spatial distribution of LAI should be affected by topographic variables (aspect, elevation, and slope), due to links between these variables and water availability effects on LAI in the sandy soils of North Florida. As such, we used a multiple regression model to remove the deterministic effects of these topographic variables prior to performing the semivariogram analysis on residual variation in LAI. Aspect, elevation, and slope were obtained from a 10 m resolution digital elevation model for each of the locations at which LAI was recorded. Because aspect is a circular variable, aspect was

decomposed into "northness" and "eastness" components with a trigonometric transformation before use in the linear model. To determine the optimal multiple regression model, all three topographic variables and their interactions were initially used, and AIC scores were then employed to ascertain which terms produced the best model. Overall, topographic variables accounted for a relatively small amount of variation in the LAI dataset (Figure 47; R^2=0.03, adjusted-R^2=0.02, $F_{5,375}$=2.45, $p<0.05$). The semivariogram analysis was performed on residual variation in LAI, and revealed that LAI measurements become spatially independent from one another at approximately 150 meters (Figure 47, bottom-right panel). Thus, ESUs should be placed at least 150 m from one another in Sandhill vegetation in order to avoid spatial oversampling.

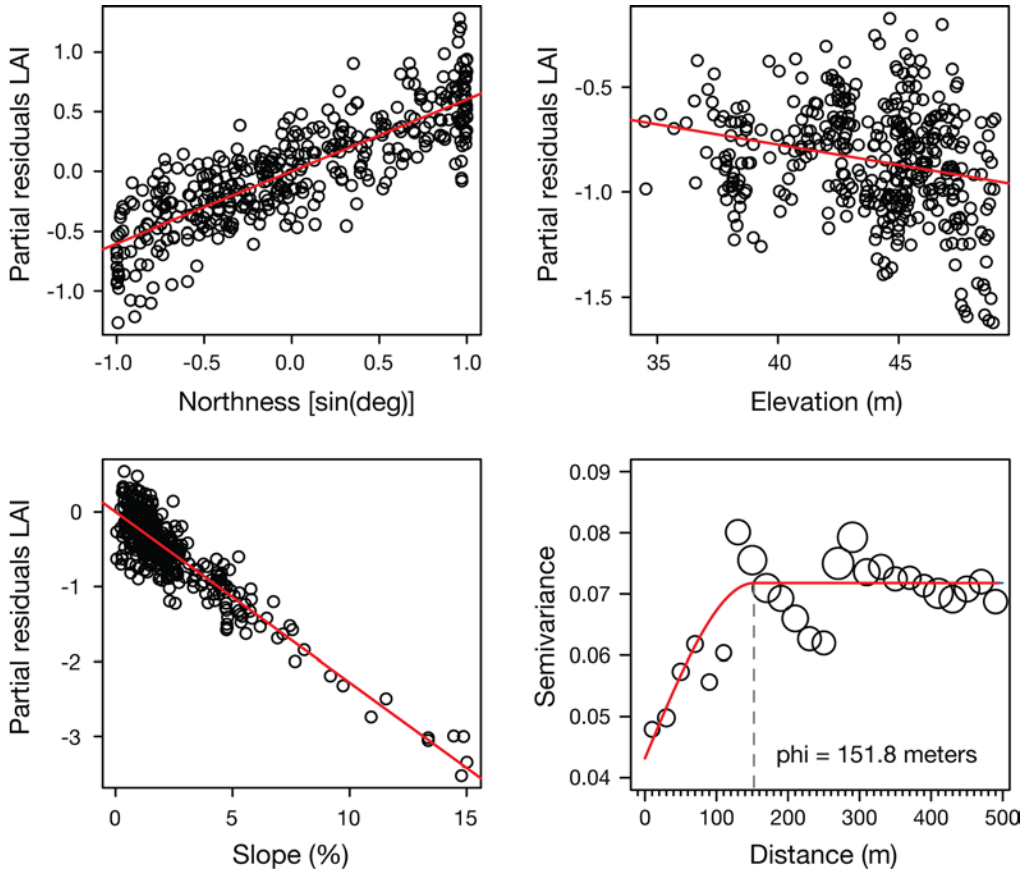

Figure 47. Partial residual plots showing influence of aspect (top-left), elevation (top-right), and slope (bottom-left) on LAI, and a semivariogram analysis on residual spatial variation in LAI (bottom-right).

7.1.8 Creation of a site-level plant biomass map: Initial steps

An important objective that requries integration of airborne remote-sensing and ground-collected datasets is creation of site-level plant biomass and net primary productivity maps. One approach to creating these maps relies on the ability to identify individual trees to species from within the remote-sensing datasets, apply species-specific allometric equations to estimate biomass, and then estimate biomass per unit area as the sum of the biomass of individual trees/shrubs within a given

pixel size. This approach depends on the ability to delineate dominant plant species from each other based on hyperspectral or vegetation structure traits that can be remotely sensed. Because only two species of trees dominate Sandhill vegetation (*P. palustris* and *Q. laevis*), this ecosystem provides an ideal opportunity to use ground-collected data (i.e. height, height to first branch, and minimum and maximum canopy diameter) that have direct remote-sensing equivalents in order to determine whether these species can be reliably identified from the air.

To determine whether *P. palustris* and *Q. laevis* could be separated based on vegetation structure alone, we performed a Principal Components Analysis (PCA) using vegetation structure data associated with only the live stems mapped and identified to species within the 20 m × 120 m plot described above and depicted in Figure 40. The results of this analysis indicate that most Pines and Oaks can be separated from each other on the basis of vegetation structure, although there is some overlap (Figure 48).

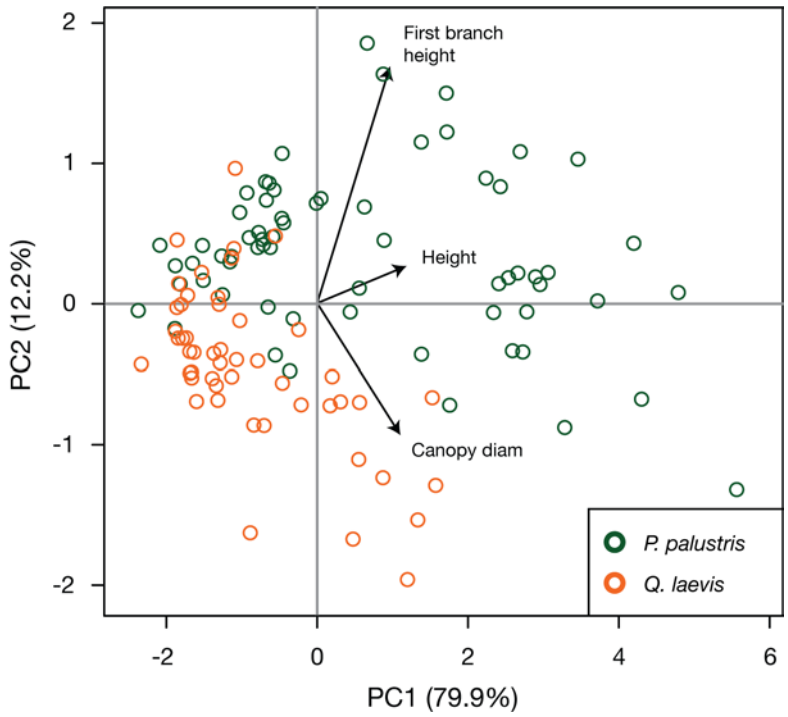

Figure 48. Principal components analysis results showing grouping of *P. palustris* and *Q. laevis* on the basis of vegetation structure measurements.

Identification of individual stems to species in plant communities with more complex species assemblages may be possible using multinomial regression models if vegetation structure traits are analyzed in conjunction with hyperspectral data that account for variation in canopy chemistry across species. If it is not possible to confidently identify individuals to species, an alternate strategy will need to be employed to generate site-level biomass maps. For example, biomass estimates could be generated at the plant community level using more general allometric equations, although it is likely that uncertainty associated with biomass estimates would increase significantly.

7.1.9 Biodiversity plot design

The campaign at Ordway-Swisher Biological Station provided the chance assess methods for measuring plant species diversity in systems of the Southeast domain, and to better understand how these measures might be integrated with the NEON airborne platform.

Even well funded projects can afford to measure only a small part a landscape[16]; most long-term observations must rely on a study design to direct sampling. We distributed twenty-six plots according to a stratified-random design. Plots were randomly located within vegetation types as described by the National Land Cover Database (NLCD). Vegetation integrates a variety of environmental gradients, and stratified random sampling increases efficiency, reduces variability, avoids oversampling common areas, and captures rare and important vegetation types[17,18]

Numerous alternatives exist for measuring plant diversity. Searching compiles species lists, but does not provide comparable metrics for monitoring purposes[19]. Historically popular techniques that rely on small transects and intercept methods for measuring plant species richness[20] are plagued by a high degree of spatial autocorrelation, a small total area sampled, a bias towards describing dominant broad-leaved species, and do not lend themselves to an understanding of patterns of diversity at larger scales[18]. Multi-scale vegetation plots detect more species for less cost, and provide comparable metrics across space, time, and monitoring networks. The size and shape of the plot typically varies based on the system and species of interest. The Ordway-Swisher prototype effort provided the opportunity to test a multi-scale circular plot to optimize plot size in several vegetation types found in the NEON Southeast domain.

We measured plant species richness and cover with a 168-m^2 multi-scale plot modified from, and directly comparable to, the Phase 3 plot of US Forest Service Forest Service Forest Inventory and Analysis Program[21,22]. In each of three 1-m^2 subplots we recorded foliar cover and average height of each species, and the cover of abiotic variables (e.g. rock, soil, standing duff, water, and wood). Species composition was recorded in a 36-m^2 subplot and across the extent of the 168-m^2 plot. At four sampling locations, we also recorded species composition in a larger, 1000-m^2 area (Figure 54).

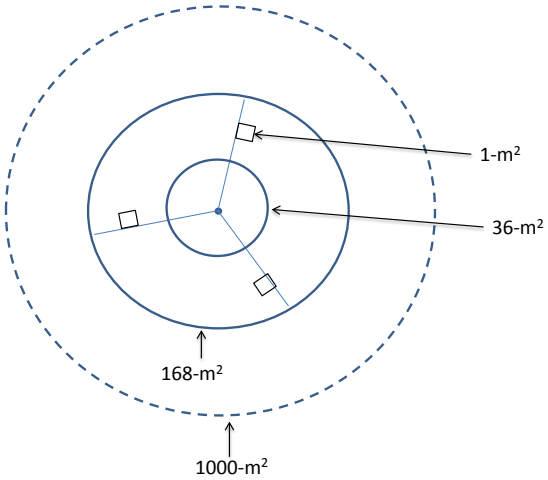

Figure 54. Multi-scale plot for sampling plant species at Ordway-Swisher Biological Station.

The sampling effort was not even across vegetation types (Table 7). Plots in the mixed evergreen deciduous forest (long-leaf pine/turkey oak) that dominate higher elevation sandy soils contained more species per plot than other vegetation types (limited to 168-m^2 plot scales, Table 1, Figure 55). Similarly, we found a greater number of total species across all plots in the mixed evergreen deciduous vegetation type than other vegetation types (Table 7).

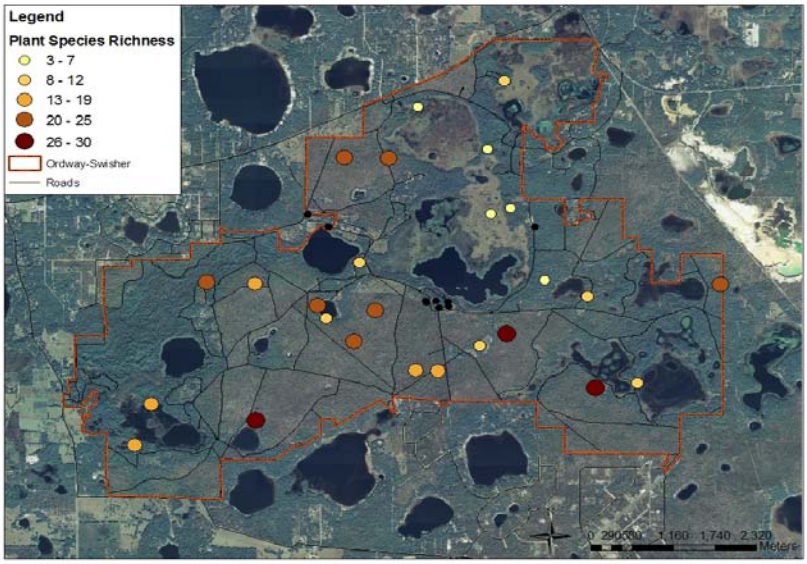

Figure 55. Location and plant species richness of plot diversity sampling.

Table 7. Vegetation as described by the NLCD types sampled at Ordway-Swisher Biological Station, the number of plots in each vegetation type, and the number of plant species per plot.

Vegetation Type	Number of Plots	Mean Species/Plot	Total Species
Deciduous Forest	4	19	81
Emergent Wetlands	5	8	44
Grassland	3	8	23
Mixed Evergreen Deciduous Forest	10	26	168
Woody Wetlands	4	14	55

To better understand the factors contributing to the patters of plant species richness across the OSBS landscape, we intersected the plant diversity sampling with a variety of landscape descriptors in a boosted regression tree environment. Independent variables were derived from Geographic Information System (GIS) landscape analyses (e.g. distance to road and water, slope, aspect), and from the NEON prototype remote sensing collection (e.g. canopy height, leaf area index, nitrogen, chlorophyll). Boosted regression trees combine machine learning and statistical techniques to split response data into homogeneous subgroups based on ranges of values of the independent predictor

variables. The approach closely resembles regression tree models; in the boosted case the performance of a single model is improved by fitting and combining many models to improve prediction. The Gradient Boosting Model (GBM) library in the R statistical package identifies the relative importance, or sensitivity index (SI) of predictor variables by measuring the number of times a variable is selected for splitting the tree and accounting for model improvement as a result of each split.

Elevation and leaf area index account for the majority of the variability in plant species richness (R^2 = 0.93, Figure 56) explained by the boosted regression tree model. We aggregated the continuous surface predictor variables to 289-m^2 grid cell resolution (17 m pixels aggregate five 3.4 m pixels) to fully encompass the 168-m^2 plot scale. Elevation was responsible for a large proportion of the explained variability (Figure 57). Small increases in elevation correspond to changes from poorly drained riparian grasslands and seasonally flooded lake margins to the deciduous and, generally at slightly higher elevation, evergreen dominated forests found on sandy soils at highest elevations of the OSBS. These forest tree species are responsible for the bulk of the leaf area index. The plant species richness response to LAI is non-linear: low values of LAI (no trees) have less richness, richness peaks at intermediate LAI, and highest values of LAI correspond to reduced richness (Figure 4). Maximum LAI values correspond to the interlocking, closed canopy of the deciduous forest. The low-light understory generally supports few species; the majority of the diversity (Table 1) is represented by the variety of canopy tree species. Alternatively, the canopy of the mixed evergreen deciduous forest is dominated, yet sparsely populated, by a single species (longleaf pine). The grass, herbaceous, and shrub species that exploit light and water under the sparse (lower LAI) canopy constitute much of the plant species richness in the mixed evergreen deciduous forest (beta diversity, Table 7), and comprise a greater proportion of the OSBS plant species richness (gamma diversity, Table 7) than the deciduous forest. While the intricacies of this conclusion might have been teased apart with a far greater number of plots and careful life-history analysis of detected species, the NEON aerial observation platform provided insight to continuous patterns of plant species richness that would likely go unnoticed.

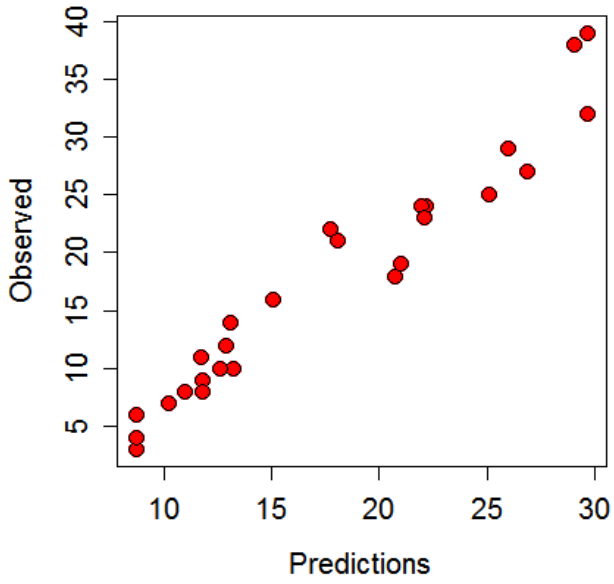

Figure 56. A K-fold cross-validation of the model guides model selection and provides an assessment of model fit by repeatedly creating subsets of the model frame and evaluating the ability of the model to predict observations of the set withheld from the model. In this case predictions were consistently lower than the observed data, but the model fit was quite good and would yield predictions with some confidence ($R^2 = 0.93$).

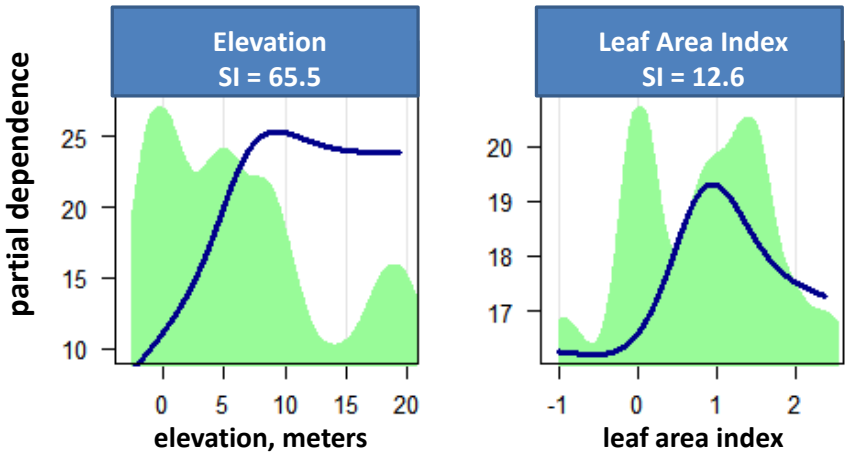

Figure 57. Partial dependence plots demonstrate the relationship between predictor variables and invasive plant species richness, the dependent variable. The green curves describe the range of variability of the dependent variable at the Ordway-Swisher Biological Station, and the blue curves describe the variability of the plant species richness with respect to the predictor variables. The sensitivity index (SI) describes the relative contribution of each predictor variable.

7.1.10 Invasive species monitoring

Invasive plant species are best detected by rigorous searching efforts that require considerable time and number of observers. The high-resolution AOP essentially searches the entire landscape. The primary goals of the invasive species prototype were to (1) describe invasive species distribution by direct detection in the NEON airborne observation data, and (2) evaluate the contribution of hyperspectral and LiDAR collections to indirect descriptions of landscape vulnerability to invasion.

Field crews mapped the location of seventy-nine invasive Pindo Palm (*Butia capitata*) individuals with high-resolution GPS units. The location, size, percent cover, and digital hemispherical photos of the individual and the canopy above the individual were recorded. At several locations the spectral signature of individuals was measured with the ASD field spectrometer.

We continue to explore direct observation of the pindo palm in the remote sensing scenes. The resulting comprehensive model of distribution across the landscape has proved challenging. The pindo palms are typically solitary individuals, many of which were small compared to the 3.4 m pixel size of the hyperspectral imagery. Isolation and identification of sub-pixel sized individuals requires algorithms 'unmix' pixel heterogeneity. Unmixing in the case of the pindo palm is challenged by the similarity of the pindo palm spectral signal to other species found at OSBS (Figure 58). Even showy individuals large enough to fill an entire pixel are difficult to detect under such circumstances. We were able to directly detect mapped pindo palm individuals in the LiDAR scenes (Figure 59), achieving some level of direct observation.

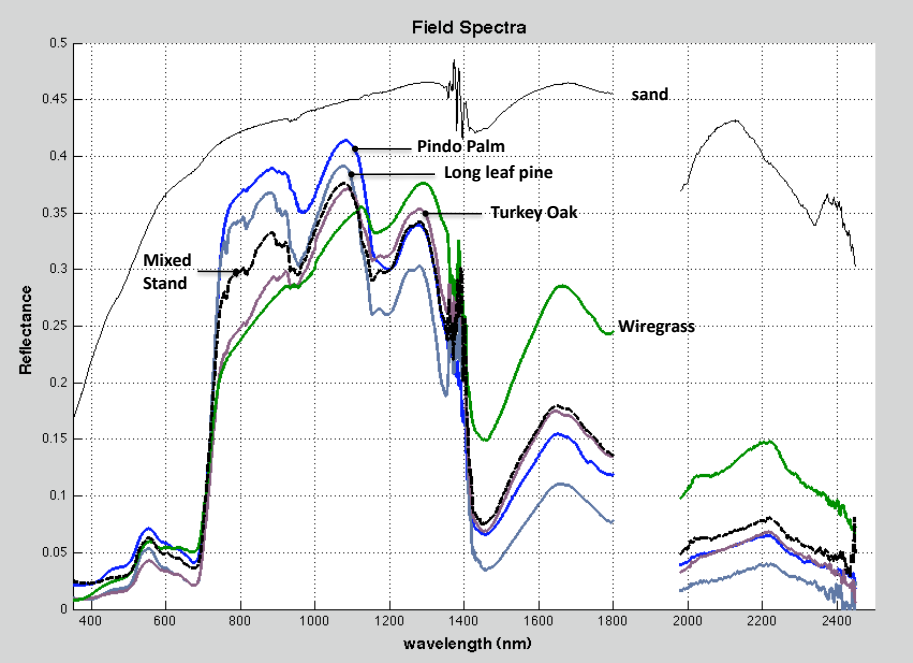

Figure 58. The spectral signal of several species at Ordway-Swisher Biological Station derived from the ASD field spectrometer.

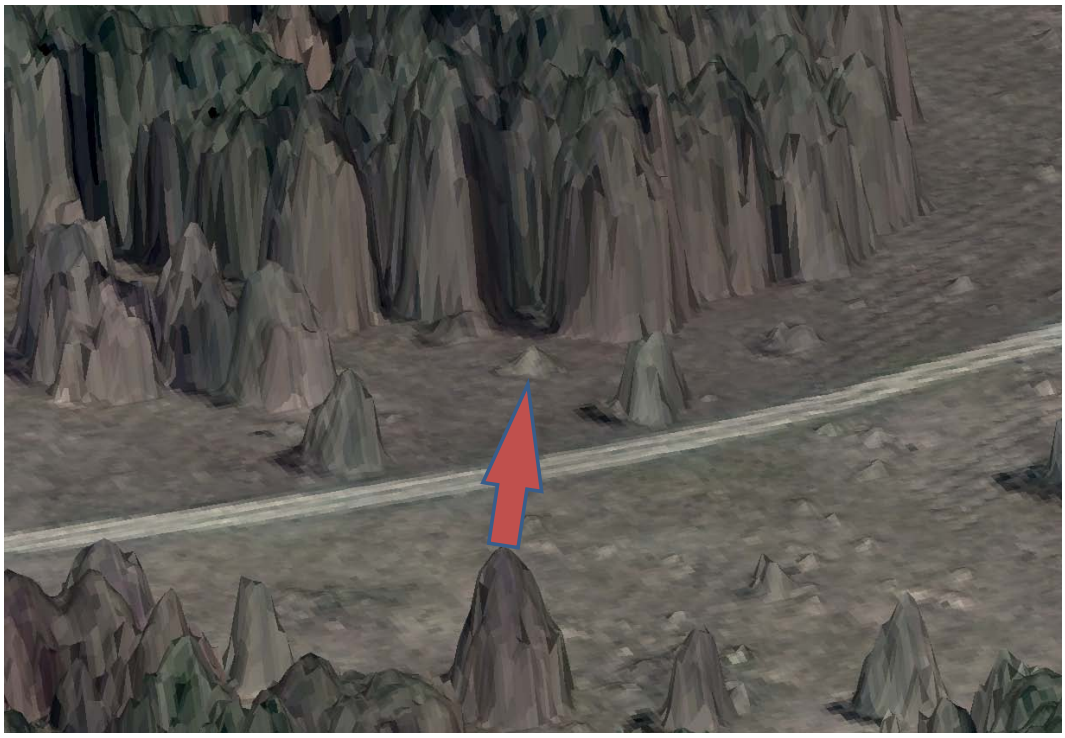

Figure 59. Direct observation of pindo palm in the LiDAR scenes from the NEON aerial observation platform. The LiDAR imagery is draped over QuickBird scene, courtesy of DigitalGlobe.

Extrapolation of mapped pindo locations provides an alternative path to understanding landscape patterns of vulnerability and invasion. Species distribution models (also called species-environmental matching models, niche models, and other names, Franklin 2009[23]) untangle the relationship of a species to the biotic and abiotic environment. The concept is to intersect mapped species locations with several environmental factors (GIS layers) to interpolate and extrapolate the probable species distribution from the sample points.

Development of species distribution modeling techniques is an active and rapidly evolving field. One popular approach, Maxent is a machine learning method (version 3.1; http://www.cs.princeton.edu/~schapire/maxent/) based on the maximum entropy principle. It estimates the probability distribution of a species by estimating the probability distribution of maximum entropy[24]. Maxent compares mapped presence locations of a species to the available environment as described by a set of background points to create a potential habitat suitability surface by projecting the relationships it finds across the entire landscape. We ran the model 25 times, withholding a different 25% of the presence locations from each model run as a test dataset for model evaluation; the final surface is an average of the 25 model runs.

We confronted known pindo palm locations with two different sets of predictor variables to assess the contribution of the AOP data to understanding patterns of landscape vulnerability: gridded surfaces derived from a variety of GIS and satellite descriptions of the landscape at a 30 m pixel size (e.g. soil, topography, vegetation), and a combination of those landscape variables and the high-

resolution data derived from the NEON airborne collection at the 17 m pixel size. Model performance as described by cross-validation was similar (area under the receiver operating curve (AUC), Figure 60). Model comparison provided evidence that the inclusion of the AOP predictor variables performed slightly better than the model limited to landscape variables (Akaike Information Criterion (AIC), Figure 60).

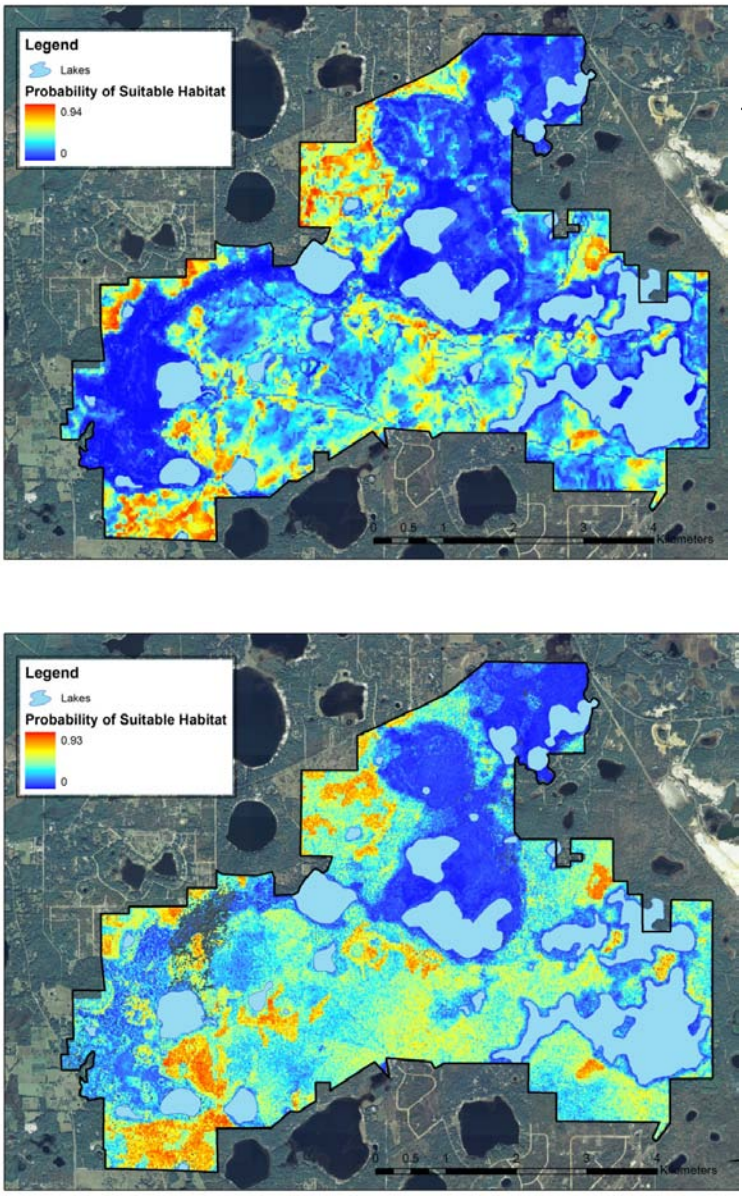

Figure 60. Competing models of pindo palm distribution. The species-habitat model that included the fine-grain hyperspectral and LiDAR data as predictor variables performed slightly better than the model that included topographic and satellite predictor variables.

We continue to evaluate how the NEON airborne data might improve invasive plant species monitoring. The species-habitat models run at the native resolution of the airborne imagery (3.4 m pixel size) did not perform as well as models that aggregate the predictor surfaces to coarser scales (17 m pixel in this analysis). The pindo palm may not respond to environmental variability at the fine-scales the airborne instrumentation can measure. We anticipate improvements to understanding of suitable habitat through iterative model optimization. Direct detection is dependent on the best, highest resolution data available. Future collection efforts with the actual NEON remote sensing package will enable spectral and LiDAR algorithm development that should further a better understanding of invasive plant species across all NEON sites.

7.2 Airborne Results

In this section we summary early findings obtained with the airborne remote sensing data including application of imaging spectroscopic data to derive estimates of biochemical parameters, estimates of leaf area index, and processing of discrete lidar returns to derive a digital surface model, a digital elevation model, and a canopy height model of the Ordway Swisher Biological Research area.

7.2.1 Spectrometer Biochemistry Results

The JPL AVIRIS data are processed at JPL using the standard AVIRIS processing approach[25]. The spectral radiance data are then processed by NEON using the Spectral Sciences, Inc. Fast Line-of-sight Atmospheric Analysis of Spectral Hypercubes (FLAASH)[26] module in the ITT Visual Information Services ENVI software to perform an atmospheric correction to determine surface spectral reflectance. This code is designed with MODTRAN to provide physical understanding behind its mathematical assumptions[27,28].

Nine spectral inversion algorithms are applied to the imagery to prototype six AOP Level 4 products including Bioclimate_004 Leaf Area Index, Biogeochemistry_009 Canopy Nitrogen, Biogeochemistry_010 Canopy Water Content, Biogeochemistry_011 Canopy Xanthophyll Cycle (PRI), Biogeochemistry_012 Canopy Chlorophyll, and Biogeochemistry_013 Canopy Lignin. A cellulose map is also generated although this is not a Level 4 product. The algorithms are coded in IDL. The IDL code calculates the spectrometer data products using the selected spectral inversion algorithms. The algorithms are chosen due to their ease of implementation and heritage in the literature[29-38]. Note that these are not the official algorithms that will generate NEON science data products but used as early prototypes.

The inversion algorithms are listed below:

NDVI, Tucker 1979 (4)

$$NDVI = \frac{R_{845} - R_{665}}{R_{845} + R_{665}}$$

LAI, Haboudane et al. 2004 (5)

$$LAI = 0.2227 * exp(3.6566 * MTVI2)$$

$$MTVI2 = \frac{1.5 * [1.2 * (R_{800} - R_{550}) - 2.5 * (R_{670} - R_{550})]}{\sqrt{(2 * R_{800} + 1)^2 - (6 * R_{800} - 5 * \sqrt{R_{670}}) - 0.5}}$$

Nitrogen, Serrano et al. 2002 (6)

$$NDNI = \frac{[log(1/R_{1510}) - log(1/R_{1680})]}{[log(1/R_{1510}) + log(1/R_{1680})]}$$

Water, Gao 1996 (7)

$$NDWI = \frac{R_{860} - R_{1240}}{R_{860} + R_{1240}}$$

Xanthophyll, Gamon et al. 1992 (8)

$$PRI = \frac{R_{570} - R_{531}}{R_{570} + R_{531}}$$

Chlorophyll, Maccioni et al. 2002 (9)

$$CHL = -11.6 + 88.56 * \left[\frac{R_{780} - R_{710}}{R_{780} + R_{680}}\right]$$

Chlorophyll, Haboudane et al. 2002 (10)

$$CHL = -30.194 * ln\left[\frac{TCARI}{OSAVI}\right] - 18.363$$
$$TCARI = 3 * [(R_{700} - R_{670}) - 0.2 * (R_{700} - R_{550}) * (R_{700}/R_{670})]$$
$$OSAVI = (1 + 0.16) * (R_{800} - R_{670})/(R_{800} + R_{670} + 0.16)$$

Lignin, Serrano et al. 2002 (11)

$$NDLI = \frac{[log(1/R_{1754}) - log(1/R_{1680})]}{[log(1/R_{1754}) + log(1/R_{1680})]}$$

Cellulose, Nagler et al. 2000 (12)

$$CAI = 0.5(R_{2000} + R_{2200}) - R_{2100}$$

A few resulting vegetation maps are shown in Figure 61.

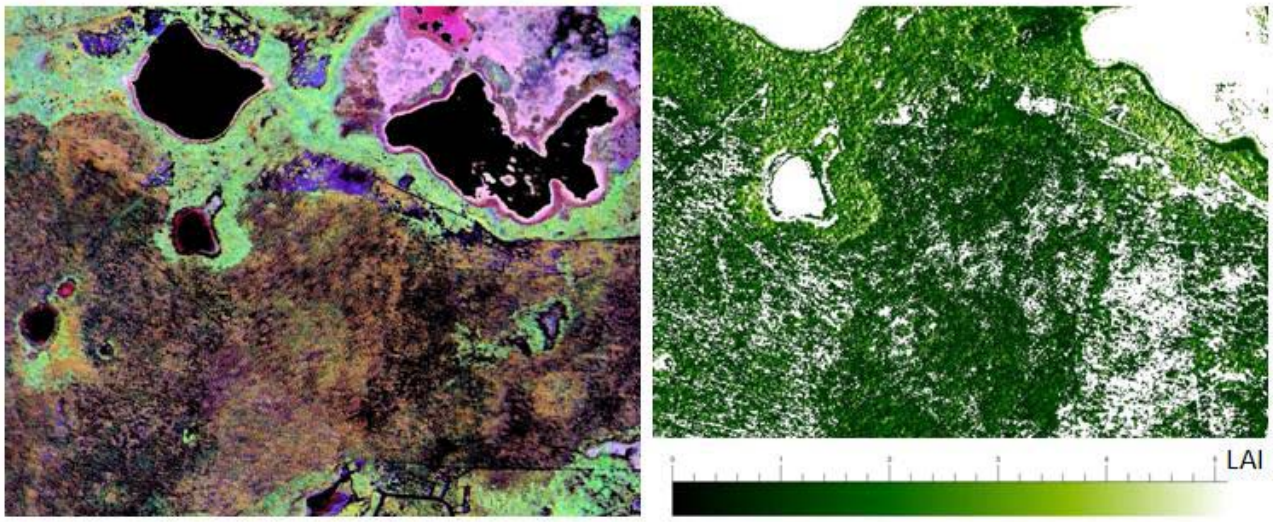

Figure 61: The left side is a false color image of OSBS with canopy water, canopy chlorophyll, and canopy nitrogen displayed in the red, green, and blue channels respectively. The right side is a LAI map of OSBS shown in shades of green.

The left image is a blow up of a section of OSBS in a false color display with canopy water displayed in the red display channel, canopy chlorophyll in the green channel, and canopy nitrogen in the blue channel. As seen in the figure, different land cover types and vegetation communities show up as distinctly different color hues. More research is required to quantify these differences in order to create a vegetation species map, or even use this information to inform the sampling strategies of the terrestrial biology team. The image on the right is a leaf area index map color coded in shades of green where dark areas have low LAI values and LAI increases with brightness. This region of OSBS encompasses the spatial area of the ground measurements of LAI performed by the terrestrial biology team. An integrated product team is currently at work investigating the differences between ground and airborne measurements of LAI and best practices for scaling these data up to coarser resolution satellite imagery products.

7.2.2 Lidar Surface Results

NCALM delivered the raw LiDAR data to NEON as part of the Pathfinder campaign. The GPS/IMU navigation data are processed by NCALM using the Applanix POSPac MMS software to determine the position, orientation, and trajectory of the aircraft. The discrete LiDAR return data are processed by NEON using the Optech DASHMap software to create point cloud data files in ASPRS LAS 1.2 format (http://www.asprs.org/society/committees/standards/asprs_las_format_v12.pdf) with a UTM GS84 projection and vertical dimension as height above ellipsoid. Each discrete return point includes information about latitude, longitude, height, intensity, and return number (multiple discrete returns can be associated with a single outgoing laser pulse). Each flight line is stored as an individual LAS file.

A basic ground finding algorithm is applied along with COTS software processing in Quick Terrain Modeler and ENVI to prototype three AOP Level 4 products including Land_Use_002 Elevation (digital elevation model DEM), Land_Use_004 Slope and Aspect, and Biodiversity_018 Ecosystem Structure (canopy height model CHM). Digital surface models (DSM) are also required in order to create the canopy height models. The ground finding algorithm[39,40] is coded in IDL. Figure 62 shows a small section of OSBS with a forested area rising up a hill just off of the southeast edge of Lake Suggs.

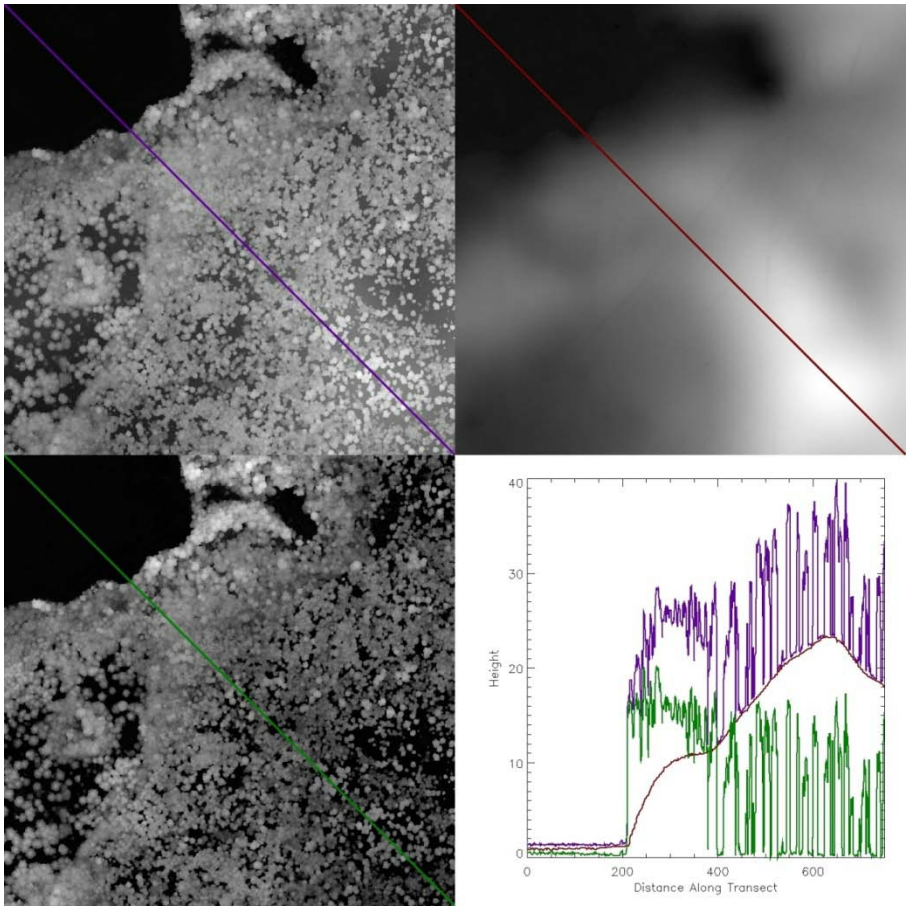

Figure 62: A digital surface model (upper left), a digital elevation model (upper right), a canopy height model (lower left), and plots of a diagonal profile through each model of an area of OSBS near Lake Suggs.

The upper left image is the DSM, the upper right is the DEM, and the lower left is the CHM. The lower right shows a plot of height versus distance along a diagonal transect across the area. The purple curve is a profile of the DSM which sits on top of the brown curve which is a profile of the DEM. Once the DEM is subtracted from the DSM, the green curve shows the residual canopy height independent of elevation. The corresponding diagonal transect is shown as a color coded line in each of the three images. The previous figure shows discrete LiDAR as gridded data, but another way to

explore the data is through visualization of the discrete point clouds, either in 3D or a 2D slice. A 2D slice along the same diagonal transect is shown in Figure 63. The top plot is the point cloud height above ellipsoid (similar to the DSM) versus the distance along the transect. In the bottom plot, the DEM heights have been subtracted from each point to arrive at height above ground (similar to the CHM). Based on the Florida Natural Areas Inventory (FNAI)[41], two distinct vegetation communities lie along this transect. Moving from left to right, the points start at Lake Suggs, at the edge of the lake exists an upland mixed forest, and then the vegetation transitions into a sandhill region. The vegetation structure appears thicker in the upland mixed forest than in the sandhill which may be a result of active fire management of the understory in the sandhill region, or may just be a natural artifact of the vegetation structure differences between the two vegetation communities. Future work will include further exploration of differences in vegetation structure seen in the LiDAR data and comparison of the canopy height model to the vegetation structure measurements performed by the terrestrial biology ground team at OSBS.

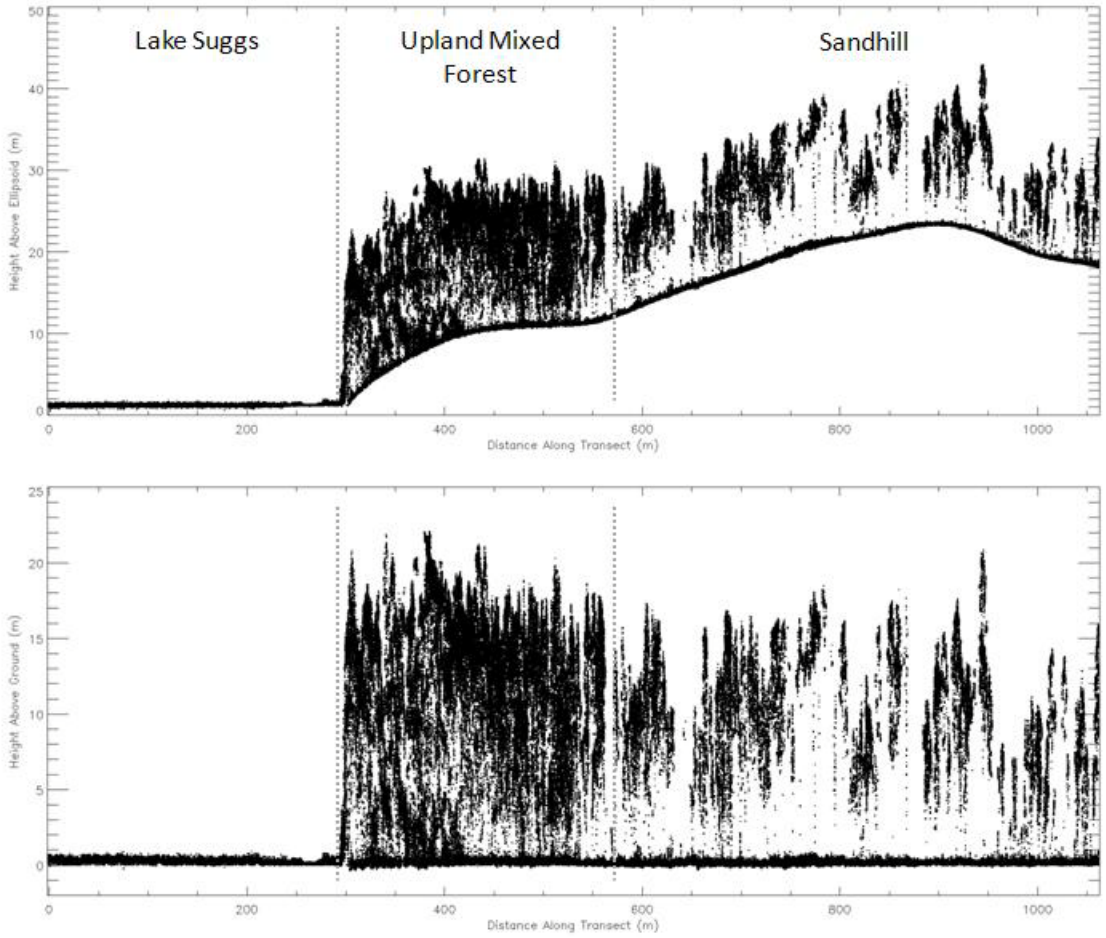

Figure 63: A 2D slice through the 3D discrete LiDAR point clouds for the diagonal transect used in Figure 8 for an area of OSBS near Lake Suggs. The top plot is the height above ellipsoid for the LiDAR points and the bottom plot shows the height above ground for the same points after the DEM has been subtracted.

A benefit of collecting coincident imaging spectrometer and LiDAR data is that vegetation chemistry as derived from the spectrometer can be analyzed in a 3D vertical structure framework, hopefully allowing more accurate or advanced analyses of ecosystem structure and function. An example of a 3D drape of a natural color QuickBird satellite image on top of the DSM is shown in Figure 64. Work is ongoing to perform similar visualizations using the vegetation chemistry prototype products and to explore the quantitative analysis of 3D vegetation structure and chemistry.

Figure 64: A 3D perspective of a natural color QuickBird satellite imagery draped over the LiDAR digital surface model

8 FUTURE WORK

8.1 Reflectance measurements

Future work to improve the NEON's capability of reflectance-based approach to vicarious calibration involves incremental improvements to several of the sections discussed above: test sites, reflectance retrieval, atmospheric characterization and radiative transfer. The most significant reason for the large variability of results found with the Pathfinder mission data is due to the non-ideal test sites. These tests were small, not uniform over large areas, and low in altitude resulting in significant atmospheric effects. This is not an issue because the typical preflight-season validation flights will be held at more ideal test sites such as Ivanpah Playa in California or Railroad Valley in Nevada.

Currently, full reference panel characterization has not been fully implemented and the factory-provided directional-hemispherical reflectance is utilized. Once added, this capability will reduce uncertainties by 1 to 2% or more.

Atmospheric characterization and radiative transfer methods implemented in commercially-available programs rely heavily on default atmospheric profiles. More realistic definition of these profiles is especially important for airborne remote sensing because unlike a space-based sensor, the view path

does not include the entire column. In addition, better characterization of adjacency effects on measured spectra, especially in regions with strong reflectance gradients, will help to improve retrievals. These issues will be a focus of development activities at NEON in the upcoming years.

Combined, it is estimated that these improvements will allow the reflectance-based method to predict at-sensor radiance to the 3-5% level of accuracy.

8.2 Spectral reflectance retrievals

The spectral reflectances derived from AVIRIS raw radiances as illustrated in Figures 37-41 show large discontinuities in spectral radiance at the edges of the water vapor bands which is indicative of incomplete water vapor correction. Further work will be undertaken, including the evaluation of alternative atmospheric correction algorithms, to improve the atmospheric correction of this data. As work progresses in this area, updated spectral reflectances will be made available on the NEON prototype web site.

8.3 Field measurements

The experience at Ordway Swisher Biological Station has provided further insight into sampling strategies for obtaining Leaf Area Index and vegetation structure measurements. Information from this Pathfinder campaign will be used to inform NEON staff in the optimization of plot/transect number, shape, size, and spacing; collection of data for prototyping plant biomass maps of sites; prototyping plot design for optimally measuring plant biodiversity within diverse ecosystem types; and optimizing the collection of ground data that will enable an initial assessment of whether airborne data can be used to monitor for presence and abundance of invasive species.

9 CONCLUSION

The 2010 NEON Pathfinder Campaign at Ordway Swisher Biological Station and Donaldson Plantation was successfully completed in September 2010. This campaign has provided pathfinder data sets that are being used effectively by the NEON Science teams to develop methods and protocols for ground site sampling, comparison between ground-based and airborne data, and data product development. This campaign has provided a baseline for establishing flight and ground-based operations in subsequent NEON airborne campaigns at NEON sites. Prototype data from the 2010 NEON Pathfinder Campaign are available from the NEON Pathfinder data website http://neoninc.org/pds/.

ACKNOWLEDGEMENTS

The National Ecological Observatory Network is a project sponsored by the National Science Foundation and managed under cooperative agreement by NEON, Inc. This material is based in part upon work supported by the National Science Foundation. Any opinions, findings, and conclusions or recommendations expressed in this material are those of the authors and do not necessarily reflect the views of the National Science Foundation.

We extend special thanks to the AVIRIS team including Michael Eastwood and J. B. Cole; the NCALM team, including Juan Carlos Fernandez, William Carter, and Ramesh Shrestha; Jeff Morrissette (USGS), who was responsible for the hemispherical camera measurements of LAI; John Hayes, Steve Coates, Rosvel Brach-Garrillo, Stephanie Spetter, Brian Johnson, Michele Kuester, Brian Damiani, and Rebecca Kao.

REFERENCES

1. Kampe, T. U., Johnson, B. R., Kuester, M., and Keller, M., “NEON: the first continental-scale ecological observatory with airborne remote sensing of vegetation canopy biochemistry and structure,” J. Appl. Rem. Sens. 4, 043510 (2010) [doi: 10.1117/1.3361375].
2. Florida Natural Areas Inventory and Florida Dept. of Natural Resources. 1990. Guide to the natural communities of Florida. Florida Natural Areas Inventory and Florida Dept. of Natural Resources, Tallahassee, FL. iv, 111 p
3. R. O. Green, M. L. Eastwood, C. M. Sarture, T. G. Chrien, M. Aronsson, B. J. Chippendale, J. A. Faust, B. E. Pavri, C. J. Chovit, M. Solis, M. R. Olah, and O. Williams, "Imaging spectroscopy and the Visible/Infrared Imaging Spectrometer (AVIRIS)," Rem. Sens. Environ. 65, 227-248 (1998).
4. M. Keller, D. S. Schimel, W. W. Hargrove, and F. M. Hoffman, "A continental strategy for the National Ecological Observatory Network," Front. Ecol. Environ. 6(5), 282-284 (2008) [doi: 10.1890/1540-9295(2008)6[282:ACSFTN]2.0.CO;2].
5. Schimel, D.S., et. al., “NEON Science Strategy: Enabling Continental Scale Ecological Forecasting,” ; available from http://www.neoninc.org/sites/default/files/NeonScienceStrategySept09.pdf, .
6. http://carboncenter.ifas.ufl.edu/ameriflux.shtml, accessed January 26, 2012.
7. http://gcmd.nasa.gov/records/GCMD_AERONET_NASA.html, accessed January 31, 2012.
8. Hoyt, D.V., “A redetermination of Rayleigh optical depth and its application to selected solar radiation problems,” J. Appl. Meteorol., Vol. 16, pp. 432-436, (1977)
9. Holben, B.N., T.F. Eck, I. Slutsker, D. Tanre, J.P. Buis, A. Setzer, J.A. Reagan, Y.J. Kaufman, T. Nakajima, F. Lavenu, I. Jankowski, A. Smirnov, “AERONET - A federated instrument network and data archive for aerosol characterization,” Rem. Sens. of Env., Vol. 66, No. 1, pp. 1-16, (1998).
10. Å̊ngström, A., “On the atmospheric transmission of sun radiation and on dust in the air,” Geografiska Annaler, Vol. 11, pp. 156-166, 1929.
11. Slater, P.N., S.F. Biggar, R.G. Holm, R.D., Jackson, Y. Mao, M.S. Moran, J.M. Palmer, B. Yuan,“Reflectance- and radiance-based methods for the in-flight absolute calibration of multispectral sensors,” Rem. Sens. Env., Vol. 22, No. 1, pp. 11-37, (1987).

12. Thome, J.K., "Absolute radiometric calibration of Landsat 7 ETM+ using the reflectance-based method," Rem. Sens. Env., 78, pp. 27-38, (2001).
13. Berk, A., L.S. Bernstein, and D.C. Robertson, "MODTRAN: A Moderate Resolution Model for LOWTRAN," Air Force Geophysics Laboratory, Air Force Systems Command, Hanscom AFB, Massachusetts, (1987).
14. Berk, A., L.S. Bernstein, G.P. Anderson, P.K. Acharya, D.C. Robertson, J.H. Chetwynd, S.M. Adler-Golden, "MODTRAN cloud and multiple scattering upgrade with application to AVIRIS," Rem. Snes. of Env., Vol. 65, No. 3, pp. 367-375, (1998).
15. M^{c}Corkel, J., "NEON ground validation capabilities for airborne and space-based imagers," NEON Technical Report NEON.DOC.000093, (2011).
16. Magurran, A. E. Ecological Diversity and Its Measurement. Princeton, NJ: Princeton University Press, 1988.
17. Muller-Dombois, D., and H. Ellenberg. Aims and Method of Vegetation Ecology. New York, NY: John Wiley & Sons, (1974).
18. Stohlgren, T. J. Measuring Plant Diversity, Lessons from the Field. New York, NY: Oxford University Press, (2007)
19. Barnett, D.T., T.J. Stohlgren, C.S. Jarnevich, G.W. Chong, J.A. Ericson, T.R. Davern, and S.A. Simonson. The art and science of weed mapping. Environmental Monitoring and Assessment 132: 235-252, (2007).
20. Barbour, M.G., J.H. Burk, and W.D. Pitts. Terrestrial Plant Ecology. Menlow Park, CA: The Benjamin/Cummings Publishing Company, (1987).
21. Bull, K.A., K.W. Stolte, and T.J. Stohlgren. Forest Health Monitoring: Vegetation Pilot Field Method Guide. Washington DC : US Forest Service, (1998).
22. Ritters, K.H., B.E. Law, R.C. Kucera, A.L. Gallant, R.L. DeVelice, and C.J. Palmer C. A selection of forest condition indicators for monitoring. Environmental Monitoring and Assessment 20:21-23, (1992).
23. Franklin, J. Mapping species distributions: spatial inference and prediction. Cambridge Univ. Press, (2009).
24. Phillips, S. J., R.P. Anderson, R.E. Schapire. Maximum entropy modeling of species geographic distributions. Ecological Modeling 190, 231-259, (2006).
25. http://aviris.jpl.nasa.gov/html/aviris.resources.html
26. Anderson, G.P., B. Pukall, C.L. Allred, L.S. Jeong, M. Hoke, J.H. Chetwynd, S.M. Adler-Golden', A. Berk, L.S. Bernstein, S.C. Richtsmeier, P.K. Acharya, and M.W. Matthew, "FLAASH and MODTRAN4: State-of-the-Art Atmospheric Correction for Hyperspectral Data," Aerospace Conference, 1999. Proceedings. 1999 IEEE , vol.4, no., pp.177-181 vol.4, 1999a, doi: 10.1109/AERO.1999.792088
27. Anderson, G.P., Alexander Berk, Prabhat K. Acharya, Michael W. Matthew, Lawrence S. Bernstein, James H. Chetwynd, Jr., H. Dothe, Steven M. Adler-Golden, Anthony J. Ratkowski, Gerald W. Felde, James A. Gardner, Michael L. Hoke, Steven C. Richtsmeier, Brian Pukall, Jason B. Mello and Laila S. Jeong, "MODTRAN4: radiative transfer modeling for remote sensing", Proc. SPIE 3866, 2 (1999b), doi:10.1117/12.371318
28. Cooley, T., Anderson, G.P. Felde, G.W. Hoke, M.L. Ratkowski, A.J. Chetwynd, J.H. Gardner, J.A. Adler-Golden, S.M. Matthew, M.W. Berk, A. Bernstein, L.S. Acharya, P.K. Miller, D.

Lewis, P. , "FLAASH, a MODTRAN4-based atmospheric correction algorithm, its application and validation," Geoscience and Remote Sensing Symposium, 2002. IGARSS '02. 2002 IEEE International , vol.3, no., pp. 1414- 1418 vol.3, (2002), doi: 10.1109/IGARSS.2002.1026134.

29. Andrew, M.E. and Ustin, S.L., "The role of environmental context in mapping invasive plants with hyperpsectral image data," Remote Sensing of Environment, 112, 4301-4317, (2008).
30. Le Maire, G., Francois, C., and Dufrene, E., "Towards universal broad leaf chlorophyll indices using PROSPECT simulated database and hyperspectral reflectance measurements," Remote Sensing of Environment, 89, 1-28, (2004).
31. Tucker, C.J., "Red and Photographic Infrared Linear Combinations for Monitoring Vegetation", Remote Sensing of Environment, 8 127-150, (1979).
32. Haboudane, D., Miller, J.R., Pattey, E., Zarco-Tejada, P.J., and Strachan, I.B., "Hyperspectral vegetation indices and novel algorithms for predicting green LAI of crop canopies: Modeling and validation in the context of precision agriculture," Remote Sensing of Environment, 90, 337-352, (2004).
33. Serrano, L., Penuelas, J., and Ustin, S.L., "Remote sensing of nitrogen and lignin in Mediterranean vegetation from AVIRIS data: Decomposing biochemical from structural signals," Remote Sensing of Environment, 81, 355-364, (2002).
34. Gao, B.-C., "NDWI A Normalized Difference Water Index for Remote Sensing of Vegetation Liquid Water From Space," Remote Sensing of Environment, 58, 257-266, (1996).
35. Gamon, J.A., Penuelas, J., and Field, C.B., "A Narrow-Waveband Spectral Index That Tracks Diurnal Changes in Photosynthetic Efficiency," Remote Sensing of Environment, 41, 35-44, (1992).
36. Maccioni, A., Agati, G., and Mazzinghi, P., "New vegetation indices for remote measurement of chlorophylls based on leaf directional reflectance spectra," Journal of Photochemistry and Photobiology B: Biology, 61, 52–61, (2001).
37. Haboudane, D., Miller, J.R., Tremblay, N., Zarco-Tejada, P.J., and Dextraze, L., "Integrated narrow-band vegetation indices for prediction of crop chlorophyll content for application to precision agriculture," Remote Sensing of Environment, 81, 416–426, (2002).
38. Nagler, P.L., Daughtry, C.S.T., and Goward, S.N., "Plant Litter and Soil Reflectance," Remote Sensing of Environment, 71, 207-215, (2000).
39. Popescu, S.C., Wynne, R.H., and Nelson, R.F., "Estimating plot-level tree heights with lidar: local filtering with a canopy-height based variable window size," Computers and Electronics in Agriculture, 37, 71-95, (2002).
40. Shan, J. and Toth, C.K., [Topographic Laser Ranging and Scanning: Principles and Processing], CRC Press, Boca Raton, FL, 590p, (2009).
41. [42] http://www.fnai.org/PDF/Natural_Communities_Guide.pdf